by NMR spectroscopy due to rapid back reaction with the CO produced in the photolysis. Studies on Fe(0) complexes of dfepe suggest that the bulky bidentate ligand is able to prevent clustering reactions of unsaturated species.[30] Thus, given the substantial Cr-alkane binding energy in (dfepe)$Cr(CO)_3$(alkane), it seems plausible that this alkane complex could be observed in NMR experiments if it could be generated in the absence of CO or other ligands capable of displacing the alkane. Experiments along these lines are planned.

(30) Brookhart, M.; Chandler, W. A.; Pfister, A. C.; Santini, C. C.; White, P. S. *Organometallics* **1992**, *11*, 1263.

Acknowledgment. We acknowledge the Gas Research Institute (Contract No. 5076-260-1596) for financial support of this work. C.C.S. acknowledges CNRS for financial support. We thank T. J. Meyer for the use of laser transient instrumentation. R.N.P. and C.H. acknowledge the support of SERC, The Royal Society, British Gas, and the European Commission. J.A.T. acknowledges the support of the Leverhulme Trust.

Electron Transfer in $Fe^{II}Fe^{III}$ Model Complexes of Iron-Oxo Proteins

Mark S. Mashuta,[†] Robert J. Webb,[‡] James K. McCusker,[‡] Edward A. Schmitt,[‡] Kenneth J. Oberhausen,[†] John F. Richardson,[†] Robert M. Buchanan,*[,†] and David N. Hendrickson*[,‡]

Contribution from the Department of Chemistry, University of Louisville, Louisville, Kentucky 40292, and the Department of Chemistry-0506, University of California at San Diego, La Jolla, California 92093-0506. *Received February 7, 1991*

Abstract: The nature of valence trapping is studied for a series of six μ-phenoxo-bis(μ-carboxylate)-bridged $Fe^{II}Fe^{III}$ complexes. The septadentate ligand $bimp^-$ binds the two metal ions and provides a phenoxide bridge as well as four imidazole moieties. The X-ray structure of $[Fe^{II}Fe^{III}(bimp)(\mu\text{-}O_2CPh)_2](BPh_4)_2\cdot{}^3/_2CH_3CN$ at 295 K is reported. This mixed-valence complex crystallizes in the $P\bar{1}$ space group with unit cell parameters of a = 15.995 (4) Å, b = 23.475 (4) Å, c = 11.464 (4) Å, α = 97.57 (1)°, β = 101.74 (1)°, γ = 85.22 (1)°, and Z = 2. A total of 11334 unique data with $I > 3\sigma(I)$ were refined to values of R = 0.045 and R_w = 0.051. The structure shows distinct octahedral (N_3O_3) high-spin Fe^{III} and Fe^{II} ions, with an Fe···Fe distance of 3.440 Å. The phenoxide Fe^{II}–O–Fe^{III} bridging angle is 115.17 (8)°. The BPh_4^- ions are not symmetrically distributed about the $Fe^{II}Fe^{III}$ cation; they are closer to the Fe^{II} ion than the Fe^{III} ion. Sharp ^1H NMR signals spanning a chemical shift range of ~350 ppm are seen for CD_3CN solutions of the $Fe^{II}Fe^{III}$ complexes. Relative to the ^1H NMR timescale these mixed-valence complexes are rapidly transferring electrons in solution. This is due to either rapid *intra*molecular electron transfer or rapid electron transfer between binuclear complexes. A weak intervalence transfer (IT) electronic absorption band is seen at ~1300 nm (ϵ = ~200 M^{-1} cm^{-1}) for all six $Fe^{II}Fe^{III}$ complexes in solution. Two quasireversible one-electron waves corresponding to the $Fe^{II}Fe^{II}/Fe^{II}Fe^{III}$ and $Fe^{II}Fe^{III}/Fe^{III}Fe^{III}$ couples are seen for each complex by cyclic voltammetry. The two waves observed for the $Fe^{II}Fe^{III}$(bimp) complexes occur at potentials 100–300 mV more negative than those reported for the analogous polypyridyl and benzimidazole complexes. Variable-temperature (5–300 K) magnetic susceptibility data are presented for two of the $Fe^{II}Fe^{III}$ complexes. These data were least-squares fit in a matrix diagonalization approach including the effects of Heisenberg magnetic exchange ($\hat{H} = -2J\hat{S}_1\cdot\hat{S}_2$), isotropic Zeeman and axial single-ion zero-field ($D\hat{S}_{z^2} - {}^1/_3S(S + 1)$] for both Fe^{II} and Fe^{III} interactions. Fitting of the data for one sample of $[Fe^{II}Fe^{III}(bimp)(\mu\text{-}O_2CCH_3)_2](ClO_4)_2\cdot 2H_2O$, for example, gave parameters of J = −3.4 cm^{-1}, $D(Fe^{II})$ = 0.63 cm^{-1}, and $g(Fe^{II})$ = 1.86. There is a $S = {}^1/_2$ ground state; however, the $S = {}^3/_2$, ${}^5/_2$, ${}^7/_2$, and ${}^9/_2$ excited states are near to the ground state. ^{57}Fe Mössbauer spectroscopy was used to thoroughly examine the temperature dependence of valence detrapping seen for the $Fe^{II}Fe^{III}$(bimp) complexes. It is shown that several of these complexes exhibit valence detrapping (onset of rapid electron transfer relative to the ^{57}Fe Mössbauer timescale) as the temperature is increased. Furthermore, there is a dependence on which anions and solvate molecules are present. Electron paramagnetic resonance (EPR) signals which are similar to those reported for the $Fe^{II}Fe^{III}$ forms of iron–oxo proteins such as hemerythrin, ribonucleotide reductase, purple acid phosphatase, and methane monooxygenase are found for liquid-helium-temperature CH_3CN solutions of the $Fe^{II}Fe^{III}$(bimp) complexes. The EPR signals are sensitive to sample conditions (frozen solution, polycrystals, etc.). The importance of the data observed for the $Fe^{II}Fe^{III}$(bimp) complexes in understanding observations on the iron–oxo proteins is discussed.

Introduction

Dinuclear oxo-bridged iron centers are known or believed to occur in the metalloproteins hemerythrin,[1-13] ribonucleotide reductase,[14-19] purple acid phosphatase,[20-24] uteroferrin,[20,25-33] and methane monooxygenase.[34-37] Hemerythrin (Hr), which is considered the prototype for this class of metalloproteins, has been shown crystallographically[5,8-10] to contain a dinuclear (μ-oxo-bis(μ-carboxylato)) iron core structure in its met form. Three histidines complete the octahedral coordination of one ferric ion while two histidines and an azide are coordinated to the second iron site in N_3-met-Hr. Ribonucleotide reductase,[14] on the other hand, has a μ-oxo-μ-carboxylato bridged Fe_2 active site and

[†] University of Louisville.
[‡] University of California at San Diego.

(1) Wilkins, P. C.; Wilkins, R. G. *Coord. Chem. Rev.* **1987**, *79*, 195-214.
(2) Klotz, I. M.; Kurtz, D. M., Jr. *Acc. Chem. Res.* **1984**, *17*, 16-22.
(3) (a) Lippard, S. J. *Angew. Chem., Int. Ed. Engl.* **1988**, *27*, 344-361. (b) Que, L., Jr. *ACS Symp. Ser.* **1988**, *No. 372*, 152-178. (c) Vincent, J. B.; Olivier-Lilley, G. L.; Averill, B. A. *Chem. Rev.* **1990**, *90*, 1447-1467.
(4) Wilkins, R. G.; Harrington, P. C. *Adv. Inorg. Biochem.* **1988**, *5*, 51-85.
(5) Klotz, I. M.; Klippenstein, G. L.; Hendrickson, W. A. *Science (Washington, D.C.)* **1976**, *192*, 335-344.
(6) Sanders-Loehr, J. In *Frontiers in Bioinorganic Chemistry*; Xavier, A. V., Ed.; VCH: Weinheim, 1986; pp 574-582.
(7) Sanders-Loehr, J.; Loehr, T. M. *Adv. Inorg. Biochem.* **1979**, *1*, 235-252.

0002-7863/92/1514-3815$03.00/0

contains imidazole, carboxylate, and water molecules as ancillary ligands. Purple acid phosphatase,[20] uteroferrin,[20,27] and methane monooxygenase[35] all have been proposed to have similar oxo-bridged diiron functional sites based on recent Mössbauer,[25,35,38-42] EPR,[1,21,23-26,34-36,39-41] magnetic susceptibility,[14,19,21,26,46,47] and EXAFS[48-52] studies.

In the diiron protein systems, the dinuclear centers exist in either a reduced (Fe_2^{II}), a mixed-valence ($Fe^{II}Fe^{III}$), or an oxidized (Fe_2^{III}) form. The ability to stabilize different oxidation states and to display reversible redox properties appears to be essential to the biological activity observed in the majority of the metalloprotein systems. Although a number of oxo-bridged dinuclear iron complexes have been reported,[53,54] most have only a single μ-oxo bridge and no μ-carboxylato bridges between the iron atoms and do not stabilize all three possible oxidation levels. Complexes of this type cannot be considered realistic protein active site analogues. More recently, several Fe_2^{III} active site model compounds[55-68] have been reported which contain μ-oxo-bis(μ-carboxylate) bridges and which duplicate the magnetic and spectral properties of met-Hr and N_3-met-Hr. In particular, Wu et al.[57] have very recently reported the synthesis and characterization of a polyimidazole Fe_2^{III} complex. Far fewer examples of Fe_2^{II} and $Fe^{II}Fe^{III}$ complexes are known.[3]

(8) Stenkamp, R. E.; Seiker, L. C.; Jensen, L. H.; Sanders-Loehr, J. *Nature* **1981**, *291*, 263-264.

(9) Stenkamp, R. E.; Seiker, L. C.; Jensen, L. H. *J. Am. Chem. Soc.* **1984**, *106*, 618-622.

(10) Stenkamp, R. E.; Seiker, L. C.; Jensen, L. H.; McCallum, J. D.; Sanders-Loehr, J. *Proc. Natl. Acad. Sci. U.S.A.* **1985**, *82*, 713-716.

(11) Kurtz, D. M., Jr.; Shriver, D.; Klotz, I. M. *Coord. Chem. Rev.* **1977**, *24*, 145-178.

(12) Stenkamp, R. E.; Jensen, L. H. *Adv. Inorg. Biochem.* **1979**, *1*, 219-233.

(13) (a) Reem, R. C.; Solomon, E. I. *J. Am. Chem. Soc.* **1984**, *106*, 8323-8325. (b) Reem, R. C.; McCormick, J. M.; Richardson, D. E.; Devlin, F. J.; Stephens, P. J.; Musselman, R. L.; Solomon, E. I. *J. Am. Chem. Soc.* **1989**, *111*, 4688-4704.

(14) (a) Sjöberg, B.-M.; Graslund, A. *Adv. Inorg. Biochem.* **1983**, *5*, 87-110. (b) Nordlund, P.; Sjöberg, B.-M.; Eklund, H. *Nature* **1990**, *345*, 593-598.

(15) Sjöberg, B.-M.; Loehr, T. M.; Sanders-Loehr, J. *Biochemistry* **1982**, *21*, 96-102.

(16) Lammers, M.; Follmann, H. *Struct. Bonding* **1983**, *48*, 133-165.

(17) Reichard, P.; Ehrenberg, A. *Science (Washington, D.C.)* **1983**, *221*, 514-519.

(18) Thelander, L.; Reichard, P. *Annu. Rev. Biochem.* **1979**, *48*, 133.

(19) Petersson, L.; Gräslund, A.; Ehrenberg, A.; Sjöberg, B.-M.; Reichard, P. *J. Biol. Chem.* **1980**, *255*, 6706-6712.

(20) (a) Antanaitis, B. C.; Aisen, P. *Adv. Inorg. Biochem.* **1983**, *5*, 111-136. (b) David, S. S.; Que, L., Jr. *J. Am. Chem. Soc.* **1990**, *112*, 6455-6463. (c) Day, E. P.; David, S. S.; Peterson, J.; Dunham, W. R.; Bonvoisin, J. J.; Sands, R. H.; Que, L., Jr. *J. Biol. Chem.* **1988**, *263*, 15561-15567.

(21) Davis, J. C.; Averill, B. A. *Proc. Natl. Acad. Sci. U.S.A.* **1982**, *79*, 4623-4627.

(22) Davis, J. C.; Lin, S. S.; Averill, B. A. *Biochemistry* **1981**, *20*, 4062-4067.

(23) Antanaitis, B. C.; Aisen, P. *J. Biol. Chem.* **1982**, *257*, 5330-5332.

(24) Que, L., Jr. *Coord. Chem. Rev.* **1983**, *50*, 73-108.

(25) Debrunner, P. C.; Hendrich, M. P.; deJersey, J.; Keough, D. T.; Sage, J. T.; Zerner, B. *Biochem. Biophys. Acta* **1983**, *745*, 103-106.

(26) Antanaitis, B. C.; Aisen, P.; Lilienthal, H. R. *J. Biol. Chem.* **1983**, *258*, 3166-3172.

(27) Antanaitis, B. C.; Aisen, P. In *Frontiers in Bioinorganic Chemistry*; Xavier, A. V., Ed.; VCH: Weinheim, 1986; pp 481-493.

(28) Antanaitis, B. C.; Peisach, J.; Mims, W. B.; Aisen, P. *J. Biol. Chem.* **1985**, *260*, 4572-4574.

(29) Antanaitis, B. C.; Aisen, P. In *Structure and Function of Iron Storage and Transport Proteins*; Urushzaki, I., Aisen, P., Listowsky, I., Drysdale, J., Eds.; Elsevier Scientific Publishing Co.: Amsterdam, 1984; p 503.

(30) Lauffer, R. B.; Antanaitis, B. C.; Aisen, P.; Que, L., Jr. *J. Biol. Chem.* **1983**, *258*, 14212-14218.

(31) Sinn, E.; O'Connor, C. J.; deJersey, J.; Zerner, B. *Inorg. Chim. Acta* **1983**, *78*, L13-L15.

(32) Keough, D. T.; Dionysius, D. A.; deJersey, J.; Zerner, B. *Biochem. Biophys. Res. Commun.* **1980**, *94*, 600-605.

(33) Buhi, W. C.; Ducsay, C. A.; Bazer, F. W.; Roberts, R. M. *J. Biol. Chem.* **1982**, *257*, 1712-1723.

(34) Woodland, M. P.; Patil, D. S.; Cammack, R.; Dalton, H. *Biochim. Biophys. Acta* **1986**, *873*, 237-242.

(35) Fox, B. G.; Sureus, K. K.; Münck, E.; Lipscomb, J. D. *J. Biol. Chem.* **1988**, *263*, 10553-10556.

(36) Woodland, M. P.; Dalton, H. *J. Biol. Chem.* **1984**, *259*, 53-59.

(37) (a) Woodland, M. P.; Cammack, R. In *Microbial Gas Metabolism*; Poole, R. K., Dow, C. S., Eds.; Academic Press: London, 1985; pp 209-213. (b) Ericson, A.; Hedman, B.; Hodgson, K. O.; Green, J.; Dalton, H.; Bentsen, J. G.; Beer, R. H.; Lippard, S. J. *J. Am. Chem. Soc.* **1988**, *110*, 2330-2332.

(38) Atkin, C. L.; Thelander, L.; Reichard, P.; Lang, G. *J. Biol. Chem.* **1973**, *248*, 7464-7472.

(39) Okamura, M. Y.; Klotz, I. M.; Johnson, C. E.; Winter, M. R. C.; Williams, R. J. P. *Biochemistry* **1969**, *8*, 1951-1958.

(40) York, J. L.; Bearden, A. J. *Biochemistry* **1970**, *9*, 4549-4554.

(41) Clark, P. E.; Webb, J. *Biochemistry* **1981**, *20*, 4628-4632.

(42) Garbett, K.; Johnson, C. E.; Klotz, I. M.; Okamura, M. Y.; Williams, R. J. P. *Arch. Biochem. Biophys.* **1971**, *142*, 574-583.

(43) Muhoberac, B. B.; Wharton, D. C.; Babcock, L. M.; Harrington, P. C.; Wilkins, P. C.; Wilkins, R. G. *Biochim. Biophys. Acta* **1980**, *626*, 337-345.

(44) Kurtz, D. M., Jr.; Sage, J. T.; Hendrich, M.; Debrunner, P.; Lukat, G. S. *J. Biol. Chem.* **1983**, *258*, 2115-2117.

(45) Martinsen, J.; Irwin, M. J.; Ho, P. S.; Hoffman, B. J.; Klotz, I. M. *Biochem. Biophys. Res. Commun.* **1983**, *112*, 954-956.

(46) Moss, T. H.; Moleski, C.; York, J. L. *Biochemistry* **1971**, *10*, 840-842.

(47) Dawson, J. W.; Gray, H. B.; Hoenig, H. E.; Rossman, G. R.; Schredder, J. M.; Wang, R. H. *Biochemistry* **1972**, *11*, 461-465.

(48) Scarrow, R. C.; Maroney, M. J.; Palmer, S. P.; Que, L., Jr.; Roe, A. L.; Salowe, S. P.; Stubbe, J. *J. Am. Chem. Soc.* **1987**, *109*, 7857-7864.

(49) Scarrow, R. C.; Maroney, M. J.; Palmer, S. M.; Que, L., Jr. *J. Am. Chem. Soc.* **1986**, *108*, 6832-6834.

(50) Elam, W. T.; Stern, E. A.; McCallum, J. D.; Sanders-Loehr, J. *J. Am. Chem. Soc.* **1982**, *104*, 6369-6373.

(51) Hendrickson, W. A.; Co, M. S.; Smith, J. L.; Hodgson, K. O.; Klippenstein, G. L. *Proc. Natl. Acad. Sci. U.S.A.* **1982**, *79*, 6255-6259.

(52) Prince, R. C.; George, G. N.; Savas, J. C.; Cramer, S. P.; Patel, R. N. *Biochim. Biophys. Acta* **1988**, *952*, 220-229.

(53) Gray, H. B.; Schugar, H. J. In *Inorganic Biochemistry*; Eichhorn, G., Ed.; Elsevier: New York, 1973; Chapter 3.

(54) Murray, K. S. *Coord. Chem. Rev.* **1974**, *12*, 1-35.

(55) (a) Armstrong, W. H.; Spool, A.; Papafthymiou, G. C.; Frankel, R. B.; Lippard, S. J. *J. Am. Chem. Soc.* **1984**, *106*, 3653-3667. (b) Armstrong, W. H.; Lippard, S. J. *Inorg. Chem.* **1985**, *24*, 981-982. (c) Hartman, J.; Rardin, R. L.; Chaudhuri, P.; Pohl, K.; Wieghardt, K.; Nuber, B.; Weiss, J.; Papafthymiou, G. C.; Frankel, R. B.; Lippard, S. J. *J. Am. Chem. Soc.* **1987**, *109*, 7387-7396.

(56) (a) Armstrong, W. H.; Lippard, S. J. *J. Am. Chem. Soc.* **1984**, *106*, 4632-4633. (b) Armstrong, W. H.; Lippard, S. J. *J. Am. Chem. Soc.* **1983**, *105*, 4837-4838.

(57) Wu, F.-J.; Kurtz, D. M.; Hagen, K. S.; Nyman, P. D.; Debrunner, P. G.; Vankai, V. A. *Inorg. Chem.* **1990**, *29*, 5174-5183.

(58) Wieghardt, K.; Pohl, K.; Ventur, D. *Angew. Chem., Int. Ed. Engl.* **1985**, *24*, 392-394.

(59) Chaudhuri, P.; Wieghardt, K.; Nuber, B.; Weiss, J. *Angew. Chem., Int. Ed. Engl.* **1985**, *24*, 778-779.

(60) Wieghardt, K.; Pohl, K.; Gebert, W. *Angew. Chem., Int. Ed. Engl.* **1983**, *22*, 727-728.

(61) Yan, S.; Cox, D. D.; Pearce, L. L.; Juarez-Garcia, C.; Que, L.; Zhang, J. H.; O'Connor, C. J. *Inorg. Chem.* **1989**, *28*, 2507-2509.

(62) Murch, B. P.; Bradley, F. C.; Que, L. *J. Am. Chem. Soc.* **1986**, *108*, 5027-5028.

(63) Murch, B. P.; Boyle, P. D.; Que, L., Jr. *J. Am. Chem. Soc.* **1985**, *107*, 6728-6729.

(64) Suzuki, M.; Oshio, H.; Uehara, A.; Kazutoyo, E.; Yanaga, M.; Kida, S.; Saito, K. *Bull. Chem. Soc. Jpn.* **1988**, *61*, 3907-3913.

(65) (a) Gomez-Romero, P.; Casan-Pastor, N.; Ben-Hussein, A.; Jameson, G. B. *J. Am. Chem. Soc.* **1988**, *110*, 1988-1990. (b) Gomez-Romero, P.; DeFotis, G. C.; James, G. B. *J. Am. Chem. Soc.* **1986**, *106*, 851-853.

(66) Vincent, J. B.; Huffman, J. C.; Christou, G.; Li, Q.; Nanny, M. A.; Hendrickson, D. N.; Fong, R. H.; Fish, R. H. *J. Am. Chem. Soc.* **1988**, *110*, 6898-6900.

(67) Toftlund, H.; Murray, K. S.; Zwack, P. R.; Taylor, L. F.; Anderson, O. P. *J. Chem. Soc., Chem. Commun.* **1986**, 191-193.

(68) Buchanan, R. M.; Oberhausen, K. J.; Richardson, J. F.; Hendrickson, D. N.; Webb, R. Manuscript in preparation.

A trapped mixed-valence configuration has been proposed for semi-met-Hr from ^1H NMR,[69] resonance Raman,[70] and EXAFS[48] studies, while a similar trapped configuration is observed for the sulfide complex from Mössbauer studies.[71] The metal centers appear to be antiferromagnetically coupled to give a $S = {}^1/_2$ ground state in semi-met-Hr.[1] Distinctive EPR signals with $g < 2$ have been observed[1,4] for mixed-valence forms of hemerythrin, purple acid phosphatase, uteroferrin, and methane monooxygenase, providing evidence of an $Fe^{II}Fe^{III}$ oxo-bridged active site. The shape and position of the EPR signals with $g < 2$ are very sensitive to subtle environmental changes of the solutions, the asymmetric nature of the coordination sphere, as well as the nature of the bridging groups at the protein sites.

We have reported previously[72] that the dinucleating polyimidazole ligand 2,6-bis[(bis(1-methylimidazol-2-yl)methyl)-amino)methyl]-4-methylphenol (Hbimp) is capable of stabilizing $Fe^{II}Fe^{III}$ mixed valence complexes of the general composition $[Fe^{II}Fe^{III}(bimp)(\mu\text{-}O_2CR)_2](X)_2$, where R = CH_3, C_2H_5, or C_6H_5 and X = ClO_4^-, BF_4^-, or $B(C_6H_5)_4^-$. Unlike the pyridine[73] and benzimidazole[74] analogues, $Fe^{II}Fe^{III}$ complexes of bimp$^-$ display valence detrapping relative to the ^{57}Fe Mössbauer timescale in the solid state over the temperature range of 100–300 K. In addition, EPR signals with $g < 2$ are observed in both solid and frozen solution samples of the $Fe^{II}Fe^{III}$ bimp complexes. In this paper are reported detailed data for a series of $Fe^{II}Fe^{III}$ mixed-valence complexes of this polyimidazole ligand to show that these complexes are good structural and electronic models of the mixed-valence site in the iron–oxo proteins.

Experimental Section

All reagents and solvents were purified and dried by standard procedures prior to use. Tetrahydrofuran (THF) was distilled from sodium benzophenone ketyl, while methanol and acetonitrile were distilled from $Mg(OCH_3)_2$ and CaH_2, respectively. The purity of all compounds was checked by TLC and ^1H and ^{13}C NMR spectroscopies. Melting points were obtained using a Hoover melting point apparatus. Microanalyses were performed by Desert Analytics, Inc., Tucson, AZ, or Galbraith Laboratory, Inc., Knoxville, TN.

Ligand Synthesis. The compounds 1-methyl-2-imidazole carboxaldehyde, 1-methyl-2-(aminomethyl)imidazole·2HCl,[73d] bis((1-methylimidazol-2-yl)methyl)amine (bmima) (**1**),[73d] and 2,6-bis(chloromethyl)-4-methylphenol (**2**)[73c] were prepared as previously described.

2,6-Bis[(bis((1-methylimidazol-2-yl)methyl)amino)methyl]-4-methylphenol [Hbimp] (3). A solution of 2,6-bis(chloromethyl)-4-methylphenol (**2**)[73c] (1.53 g, 7.5 mmol) in 50 mL of tetrahydrofuran (THF) was added slowly to a solution of **1** (3.09 g, 15.0 mmol) and triethylamine (2.4 g, 24.0 mmol) in 175 mL of THF. The resulting solution was allowed to stir for 4 h and the precipitate filtered and washed with 10 mL of THF. The filtrate and washings were taken to dryness under reduced pressure and the crude oil was dissolved in 20 mL of water. The solution was made alkaline with $KHCO_3$ and then extracted with 3 × 50 mL portions of CH_2Cl_2. The extracts were combined, washed with a saturated NaCl solution, and the CH_2Cl_2 dried with $MgSO_4$. The CH_2Cl_2 was then removed under reduced pressure to give 1.96 g (48%) of compound **3**. Anal. Calcd (found) for $C_{29}H_{38}N_{10}O$: C, 64.18 (63.89); H, 7.06 (7.27); N, 25.81 (24.78). ^1H NMR ($CDCl_3$) 2.20 (s, 3 H), 3.30 (s, 12 H), 3.69 (s, 4 H), 3.70 (s, 8 H), 6.76 (s, 4 H), 6.83 (s, 2 H), 6.90 (s, 4 H).

Synthesis of Metal Complexes. Mixed-valence complexes were prepared using either method 1 or 2.

Method 1. $[Fe^{II}Fe^{III}(bimp)(\mu\text{-}O_2CCH_3)_2](ClO_4)_2\cdot 2H_2O$ (**4**) was prepared by reacting 0.54 g (1 mmol) of Hbimp and 0.169 g (2 mmol) of sodium acetate dissolved in 20 mL of methanol with 0.79 (2 mmol) of $Fe(ClO_4)_2\cdot 6H_2O$ dissolved in 10 mL of methanol. The resulting brown-purple solution was stirred for 12 h, whereupon a brown precipitate was isolated by filtration. The complex was recrystallized from a 1:1 acetonitrile/toluene solution, mp > 300 °C (dec). Anal. Calcd (found) for $Fe_2C_{33}H_{47}N_{10}Cl_2O_{15}$: C, 39.38 (38.81); H, 4.71 (4.65); N, 13.91 (14.11); Cl, 7.04 (7.05); Fe, 11.11 (11.07).

Electronic spectral data [CH_3CN, λ_{max} (nm), ϵ_{Fe} (M^{-1} cm^{-1})]: 306 (1100), 375 (690), 523 (660), 960 (170), 1332 (180). ^1H NMR (CD_3CN, δ): 7.05 (s, 6 H) [Im-CH_3], 13.38 (s, 6 H) [Im-CH_3], 54.18 (s, 2 H) [m-ArH], 55.85 (s, 2 H) [ImH], 56.47 (s, 2 H) [ImH], 57.94 (s, 2 H) [$ImCH_2$], 65.68 (s, 3 H) [$ArCH_3$], 67.26 (s, 6 H) [acetate CH_3], 79.61 (s, 2 H) [ImH], 80.40 (s, 2 H) [$ImCH_2$]; 85.21 (s, 2 H) [ImH], 90.72 (s, 2 H) [$ArCH_2$], 174.76 (s, 2 H) [$ImCH_2$], 214.01 (s, 2 H) [$ImCH_2$] 342.05 (s, 2 H) [$ArCH_2$].

$[Fe^{II}Fe^{III}(bimp)(\mu\text{-}O_2CCH_2CH_3)_2](ClO_4)_2\cdot 2H_2O$ (**5**) was prepared in a similar manner to compound **2** except 0.19 g (2 mmol) of sodium proprionate and 0.54 g (1 mmol) of Hbimp were added dropwise to a methanol solution containing 0.79 g (2 mmol) of $Fe(ClO_4)_2\cdot 6H_2O$. The resulting brown purple solution was stirred for 9 h, whereupon the complex precipitated from solution. The precipitate was isolated by filtration yielding 0.74 g (75%) of a dark brown solid that was recrystallized from acetonitrile/toluene. Slow evaporation of the solvent under a stream of dry nitrogen afforded small brown-purple crystals which were found to twin readily, mp > 300 °C (dec). Anal. Calcd (found) for $Fe_2C_{35}H_{51}N_{10}O_{15}Cl_2$: Fe, 10.81 (10.80); C, 40.63 (40.13); H, 4.97 (4.72); N, 13.53 (13.19). Electronic spectral data [CH_3CN, λ_{max} (nm), ϵ_{Fe} (M^{-1} cm^{-1})]: 305 (1100), 375 (680), 523 (650), 960 (170), 1331 (180). ^1H NMR (CD_3CN, δ) 6.95 (s, 6 H) [$ImCH_3$], 13.20 (s, 6 H) [$ImCH_3$], 20.35 (s, 6 H) [proprionate CH_3], 40.62 (s, 2 H) [proprionate CH_2], 55.68 (s, 2 H) [ArH], 56.03 (s, 2 H) [ImH], 56.45 (s, 2 H) [ImH], 57.25 (s, 2 H) [$ImCH_2$], 66.10 (s, 2 H) [proprionate CH_2], 67.05 (s, 3 H) [$ArCH_3$], 80.23 (s, 2 H) [ImH], 81.27 (s, 2 H) [$ImCH_2$], 86.40 (s, 2 H) [ImH], 90.60 (s, 2 H) [$ArCH_2$], 174.70 (s, 2 H) [$ImCH_2$], 214.00 (s, 2 H) [$ImCH_2$], 342.00 (s, 2 H) [$ArCH_2$].

$[Fe^{II}Fe^{III}(bimp)(\mu\text{-}O_2CPh)_2](ClO_4)_2\cdot 2H_2O$ (**6**) was prepared following the same procedure as described above except 0.29 g (2 mmol) of sodium benzoate was used instead of sodium acetate or sodium proprionate. Recrystallization of the complex from acetonitrile/toluene yielded 0.63 g (58%) of a microcrystalline sample, mp > 300 °C (dec). Anal. Calcd (found) for $Fe_2C_{45}N_{10}O_{15}Cl_2$: Fe, 9.65 (9.48); C, 46.65 (47.11); H, 4.78 (4.74); N, 12.08 (12.02). Electronic spectral data [CH_3CN, λ_{max} (nm), ϵ_{Fe} (M^{-1} cm^{-1})]: 307 (1100), 375 (690), 523 (670), 961 (180), 1331 (190).

$[Fe^{II}Fe^{III}(bimp)(\mu\text{-}O_2CCH_3)_2](BF_4)_2\cdot 2H_2O$ (**7**). A methanol solution containing 0.27 g (0.5 mmol) of Hbimp and 0.09 (2 mmol) of sodium acetate was added slowly to a methanol (20 mL) solution containing 0.33 g (2 mmol) of $Fe(BF_4)_2\cdot 6H_2O$. The purple reaction mixture was stirred for several hours and filtered giving 0.34 g (65%) of a brown solid. Compound **7** was dissolved in a minimal amount of acetonitrile and layered with toluene. Slow evaporation of the solvent under an inert atmosphere gave brown purple crystals, mp > 300 °C (dec). Anal. Calcd (found) for $Fe_2C_{33}H_{49}N_{10}B_2F_8O_6$: C, 41.04 (41.19); H, 5.08 (4.98); N, 14.51 (14.23).

$[Fe^{II}Fe^{III}(bimp)(\mu\text{-}O_2CCH_2CH_3)_2](BPh_4)_2\cdot 2CH_3CN$ (**8**) was prepared in a manner similar to above except sodium tetraphenylborate was used to precipitate the complex (54%). The dark purple solid was recrystallized from acetonitrile, mp > 300 °C (dec). Electronic spectral data [CH_3CN, λ_{max} (nm), ϵ_{Fe} (M^{-1} cm^{-1})]: 306 (1100), 375 (690), 523 (660), 960 (170), 1332 (180).

$[Fe^{II}Fe^{III}(bimp)(\mu\text{-}O_2CPh)_2](BPh_4)_2\cdot {}^3/_2CH_3CN$ (**9**) was prepared by the same method used to prepare compound **7** except sodium benzoate was substituted for sodium acetate. The complex was recrystallized from acetonitrile by slow evaporation of the solvent under a dry nitrogen atmosphere affording crystals suitable for X-ray structural analysis, mp > 300 °C (dec). Anal. Calcd (found) for $Fe_2C_{94}H_{91.5}N_{11.5}B_2O_5$: C, 70.75 (71.07); H, 5.76 (5.94); N, 10.13 (10.14); Fe, 7.00 (7.04). Electronic spectral data [CH_3CN, λ_{max} (nm), ϵ_{Fe} (M^{-1} cm^{-1})]: 305 (110), 375 (680), 523 (660), 961 (180), 1331 (190).

Method 2. This method involves a two-step metalation of the bimp$^-$ ligand identical to that used in preparing a series of heterobimetallic polyimidazole complexes.[75] A monometalated Fe^{III}(bimp) complex (**10**)

(69) Maroney, M. J.; Kurtz, D. M., Jr.; Noeck, J. M.; Pearce, L. L.; Que, L., Jr. *J. Am. Chem. Soc.* **1986**, *108*, 6871–6879.
(70) Irwin, M. J.; Duff, L. L.; Shriver, D. F.; Klotz, I. M. *Arch. Biochem. Biophys.* **1983**, *224*, 473–478.
(71) Kurtz, D. M., Jr.; Sage, J. T.; Hendrich, M.; Debrunner, P.; Lukat, G. S. *J. Biol. Chem.* **1988**, *258*, 2115–2117.
(72) Mashuta, M. S.; Webb, R. J.; Oberhausen, K. J.; Richardson, J. F.; Buchanan, R. M.; Hendrickson, D. N. *J. Am. Chem. Soc.* **1989**, *111*, 2745–2746.
(73) (a) Borovik, A. S.; Murch, B. P.; Que, L., Jr.; Papaefthymiou, V.; Münck, E. *J. Am. Chem. Soc.* **1987**, *109*, 7190–7191. (b) Borovik, A. S.; Papaefthymiou, V.; Taylor, L. F.; Anderson, O. P.; Que, L., Jr. *J. Am. Chem. Soc.* **1989**, *111*, 6183–6195. (c) Borovik, A. S.; Que, L., Jr. *J. Am. Chem. Soc.* **1988**, *110*, 2345–2347. (d) Oberhausen, K. J.; Richardson, J. F.; Pierce, W.; Buchanan, R. M. *Polyhedron* **1989**, *8*, 659–668.
(74) (a) Suzuki, M.; Uehara, A.; Hiroki, O.; Kazutoyo, E.; Yanaga, M.; Kida, S.; Saito, K. *Bull. Chem. Soc. Jpn.* **1987**, *60*, 3547–3555. (b) Suzuki, M.; Uehara, A.; Endo, K. *Inorg. Chim. Acta* **1986**, *123*, L9–L10. (c) Suzuki, M.; Murata, S.; Uehara, A.; Kida, S. *Chem. Lett.* **1987**, 281–284. (d) Karlin, K. D.; Dahlstrom, P. L.; Cozzette, S. N.; Scensay, P. M.; Zubieta, J. *J. Chem. Soc., Chem. Commun.* **1981**, 881–882.

(75) Buchanan, R. M.; Mashuta, M. S.; Richardson, J. F.; Webb, R. J.; Oberhausen, K. J.; Nanny, M. A.; Hendrickson, D. N. *Inorg. Chem.* **1990**, *29*, 1299–1301.

Table I. Crystallographic Data for $[Fe^{II}Fe^{III}(bimp)(O_2CPh)_2](BPh_4)_2 \cdot {}^3/_2CH_3CN$

formula	$C_{94}H_{91.5}B_2Fe_2N_{11.5}O_5$
formula weight	1595.65
space group	$P\bar{1}$
a, Å	15.995 (4)
b, Å	23.475 (4)
c, Å	11.464 (4)
α, deg	97.57 (1)
β, deg	101.74 (1)
γ, deg	85.22 (1)
vol, Å^3	4170.8
Z	2
D_c, g/cm^3	1.27
radiation (λ, nm)	Mo Kα (0.71073)
monochromator	graphite
scan range	1.5 (0.80 + 0.34 tan θ)
scan speed, deg min^{-1}	1 to 3
no. of unique reflcns collctd	14638
crystal dimens, mm	0.4 × 0.4 × 0.3
μ(Mo Kα), cm^{-1}	4.0
min/max trans coeff	0.910, 0.998
weighting formula	$[\sigma(F)^2 + (0.03F)^2 + 2.0]^{-1}$
no. of variables	1021
no. of observns ($I > 3\sigma(I)$)	11334
max Δ/σ	0.70
GOF	2.38
agreement factors: R^a	0.045
$R_w^{b,c}$	0.051

$^a R = \sum(|F_o| - |F_c|)/\sum|F_o|$. $^b R_w = [\sum w(|F_o| - |F_c|)^2/\sum w|F_o|^2]^{1/2}$. $^c w = [\sigma(F)^2 + (0.02F)^2 + 2.0]^{-1}$.

has been used to prepare compounds **4–9** as described below.

(Acetato)(2,6-bis[bis(((1-methylimidazol-2-yl)methyl)amino)-methyl])(4-methylphenolato)iron(III) perchlorate (**10**). Compound **10** was prepared by mixing a methanol solution containing 0.54 g (1 mmol) of Hbimp and 0.09 (1 mmol) of sodium acetate with 0.46 g (1 mmol) of $Fe(ClO_4)_3 \cdot 6H_2O$ dissolved in methanol. After the mixture was stirred at 25 °C for 12 h, the complex precipitated, was isolated by filtration, and dried at room temperature in vacuo. Compound **10** was recrystallized from methylene chloride/hexane solution. Anal. Calcd (found) for $FeC_{31}H_{40}N_{10}O_7Cl$: C, 49.26 (48.90); H, 5.33 (5.45); N, 18.52 (18.15); Fe, 7.38 (7.32). Electronic spectral data [CH_3CN; λ_{max} (nm), ϵ_{Fe} (M^{-1} cm^{-1})]: 313 (2800), 329 (1300), 559 (670).

Compounds **4–9** were prepared as follows: addition of 1 mmol of compound **10** dissolved in 5 mL of methanol was added to a methanol solution of 1 mmol of $Fe(ClO_4)_2 \cdot 9H_2O$ containing an excess amount of appropriate sodium carboxylate and either $NaClO_4$, $NaBF_4$, or $NaB(C_6H_5)_4$. The desired $Fe^{II}Fe^{III}$ complexes precipitated after several hours and were isolated by filtration. All samples gave satisfactory analyses.

Crystallographic Results for $[Fe^{II}Fe^{III}(bimp)(\mu\text{-}O_2CPh)_2](BPh_4)_2 \cdot 1.5CH_3CN$ (9). A brown-purple crystal of compound **9** was mounted on a glass fiber and coated with epoxy to retard possible solvent loss. Data were collected at 295 K on an Enraf-Nonius CAD-4-diffractometer using the ω–2θ scan technique to a maximum $2\theta = 50°$. Unit cell parameters were obtained by least-squared refinement of 25 accurately centered reflections having $15 < 2\theta < 18°$ and the choice of space group was confirmed by the program TRACER[76] and by the successful solution of the structure. All pertinent crystallographic data can be found in Table I. The stability of the crystal was monitored every hour using three standard reflections. No significant decay in the intensities of these reflections was observed. All data were corrected for Lorentz and polarization effects and an empirical absorption correction based on ψ scans was applied. The relative transmission coefficient ranged from 0.904 to 1.000. Scattering factors were taken from Cromer and Weber[77] and anomalous dispersion effects were included in F_c.[78]

The positions of the iron atoms were determined using direct methods (MULTAN) and the remaining non-hydrogen atoms were located from a series of difference Fourier maps. Hydrogen atoms were included in ideal positions in the final refinement cycle as fixed contributions (C–H = 1.00 Å, $B_{iso} = 1.2B$ of the bonded atom) to the structure factors. The model was refined using full-matrix least-squares techniques based on F. Both Fe atoms were refined using scattering factors for Fe^{II}. The smaller value for B_{eq} of Fe(1) is consistent with it being an Fe^{III} center (vide infra). Selected bond lengths and angles are given in Table II. Anisotropic thermal parameters, hydrogen atom positional parameters, and a listing of structure factors have been deposited as supplementary material.

Physical Methods. Visible and near-IR electronic absorption spectra of the complexes were recorded on Shimatzu Model 160 and Perkin-Elmer spectrophotometers. All solutions were prepared in CH_3CN in an inert atmosphere glovebox under nitrogen. ^1H NMR spectra of the mixed-valence complexes were obtained on Varian XL 300-MHz and Brüker 500-MHz spectrometers. Solutions were prepared using degassed CD_3CN (~5 mM in complex). X-band (9.03 GHz) EPR spectra were obtained on a Varian E-109 spectrometer equipped with an Oxford Instruments helium cryogenic system. Frozen solution spectra were obtained using thoroughly degassed acetonitrile. Mössbauer spectra were obtained on a constant acceleration instrument which has been described previously.[79] Magnetic susceptibility data were recorded on a Model VTS-900 SQUID susceptometer (BTi, Inc., San Diego, CA) in an applied field of 10.00 kG. Temperature control was achieved using a BTi digital temperature control device. Diamagnetic corrections were estimated from Pascal's constants.[80]

Electrochemical studies were performed using a PARC Model 174 universal programmer, Model 175 potentiostat/galvanostat, and Model 178 digital coulometer. All electrochemical measurements were performed in an inert atmosphere glovebox under nitrogen using degassed acetonitrile solutions (distilled from CaH_2) with 0.1 M tetrabutylammonium perchlorate as the supporting electrolyte. Cyclic voltammograms were obtained using a three-component electrochemical cell. The working electrode consisted of a platinum wire electrode while the reference and auxiliary electrodes were Ag/AgCl and a platinum coil, respectively. The ferrocene/ferrocenium redox couple was used as an external standard.

Results and Discussion

Compound Synthesis. A series of triply bridged dinuclear complexes of the polyimidazole ligand 2,6-bis[bis(((1-methylimidazol-2-yl)methyl)amino)methyl]-4-methylphenol (Hbimp) has been prepared. This ligand is one of only a few known polyimidazole ligands.[81] Reaction of 2,6-bis(chloromethyl)-*p*-cresol (**1**) with bis((1-methylimidazol-2-yl)methyl)amine (**2**) in THF solutions containing excess triethylamine affords Hbimp (**3**). The resulting triethylamine hydrochloride can be removed by filtration and the excess triethylamine and solvent removed in vacuo to give a crude oil of **3**. The oil crystallizes from a mixture of THF/hexane giving compound **3** as a white solid. Mixed valence

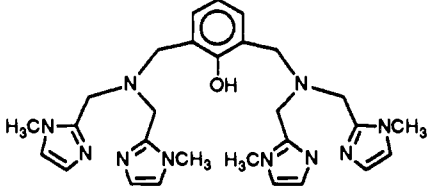

3

$Fe^{II}Fe^{III}$ complexes having the general composition $[Fe^{II}Fe^{III}$-

(76) Frenz, B. A. The Enraf-Nonius CAD 4 SDP—a real-time system for concurrent X-ray data collection and crystal structure determination. In Schenk, H., O Hhof Hazekamp, R., vanKoningsveld, H., Bassi, G. C., Eds.; *Computing in Crystallography*; Delft University Press: Delft, The Netherlands, 1978; pp 64–71.

(77) Cromer, D. T.; Weber, J. T. *International Tables for X-ray Crystallography*; Kynoch Press: Birmingham, UK, 1974; Vol. IV, Table 2.2.3.

(78) Cromer, D. T. *International Tables for X-ray Crystallography*; Kynoch Press: Birmingham, UK, 1974; Vol. IV, Table 2.3.1.

(79) Cohn, M. J.; Timken, M. D.; Hendrickson, D. N. *J. Am. Chem. Soc.* **1984**, *106*, 6683–6689.

(80) *Theory and Applications of Molecular Paramagnetism*; Boudreaux, E. A., Mulay, L. N., Eds.; J. Wiley and Sons, Inc.: New York, 1976.

(81) (a) Tang, C. C.; Davalian, D.; Huang, P.; Breslow, R. *J. Am. Chem. Soc.* **1978**, *100*, 3918–3922. (b) Breslow, R.; Tarnowski, T. *J. Am. Chem. Soc.* **1983**, *105*, 5337–5342. (c) Brown, R. S.; Huguet, J. *Can. J. Chem.* **1980**, *58*, 889–901. (d) Slebocka-Tilk, H.; Cocho, J. L.; Frakman, Z.; Brown, R. S. *J. Am. Chem. Soc.* **1984**, *106*, 2421–2431. (e) Sorrell, T. N.; Borovik, A. S. *J. Am. Chem. Soc.* **1986**, *108*, 2479–2481. (f) Gorun, S. M.; Lippard, S. J. *Inorg. Chem.* **1988**, *27*, 149–156. (g) Potvin, P. G.; Wong, M. H. *J. Chem. Soc., Chem. Commun.* **1987**, 672–674. (h) Tolman, W. B.; Rardin, R. L.; Lippard, S. J. *J. Am. Chem. Soc.* **1989**, *111*, 4532–4533. (i) Traylor, T. G.; Hill, K. W.; Tian, Z-Q.; Rheingold, A. L.; Peisach, J.; McCracken, J. *J. Am. Chem. Soc.* **1988**, *110*, 5571–5572. (j) Divaira, M.; Mani, F.; Stopploni, P. *Cun. Chem. React.* **1989**, *11*, 127–129. (k) Beer, R. H.; Tolman, W. B.; Bott, S. G.; Lippard, S. J. *Inorg. Chem.* **1989**, *28*, 4557–4559. (l) Mulliez, E. *Tetrahedron Lett.* **1989**, *20*, 6169–6172.

Table II. Selected Bond Distances (Å) and Angles (deg) for $[Fe^{II}Fe^{III}(bimp)(O_2CPh)_2](BPh_4)_2 \cdot {}^3/_2CH_3CN$

atom 1	atom 2	distance	atom 1	atom 2	distance	atom 1	atom 2	distance
Fe(1)	O(1)	1.958 (2)	N(1)	C(8)	1.494 (3)	N(7)	C(22)	1.371 (5)
Fe(1)	O(2)	1.944 (2)	N(1)	C(10)	1.487 (4)	N(8)	C(21)	1.339 (4)
Fe(1)	O(4)	2.017 (2)	N(1)	C(15)	1.486 (4)	N(8)	C(23)	1.374 (5)
Fe(1)	N(1)	2.264 (2)	N(2)	C(11)	1.327 (4)	N(8)	C(24)	1.469 (6)
Fe(1)	N(2)	2.105 (2)	N(2)	C(12)	1.385 (4)	N(9)	C(26)	1.318 (4)
Fe(1)	N(4)	2.088 (2)	N(3)	C(11)	1.338 (3)	N(9)	C(27)	1.379 (5)
Fe(2)	O(1)	2.115 (2)	N(3)	C(13)	1.375 (4)	N(10)	C(26)	1.332 (4)
Fe(2)	O(3)	2.129 (3)	N(4)	C(16)	1.333 (4)	N(10)	C(28)	1.382 (5)
Fe(2)	O(5)	2.076 (3)	N(4)	C(17)	1.400 (5)	N(10)	C(29)	1.469 (6)
Fe(2)	N(6)	2.301 (2)	N(5)	C(16)	1.330 (5)	N(110)	C(111)	1.117 (8)
Fe(2)	N(7)	2.125 (3)	N(5)	C(18)	1.396 (5)	N(120)	C(121)	0.98 (3)
Fe(2)	N(9)	2.123 (3)	N(5)	C(19)	1.468 (5)	C(111)	C(112)	1.440 (9)
O(1)	C(1)	1.364 (3)	N(6)	C(9)	1.483 (3)	C(121)	C(122)	0.93 (4)
O(2)	C(30)	1.287 (3)	N(6)	C(20)	1.477 (5)	C(1)	C(2)	1.395 (4)
O(3)	C(30)	1.232 (3)	N(6)	C(25)	1.483 (4)	C(1)	C(6)	1.395 (4)
O(4)	C(37)	1.246 (4)	N(7)	C(21)	1.323 (4)	C(2)	C(3)	1.393 (4)
O(5)	C(37)	1.257 (4)						

atom 1	atom 2	atom 3	angle	atom 1	atom 2	atom 3	angle
O(1)	Fe(1)	O(2)	101.91 (9)	O(3)	Fe(2)	O(5)	94.9 (2)
O(1)	Fe(1)	O(4)	90.94 (8)	O(3)	Fe(2)	N(6)	96.20 (9)
O(1)	Fe(1)	N(1)	88.25 (7)	O(5)	Fe(2)	N(7)	102.4 (2)
O(1)	Fe(1)	N(2)	162.08 (9)	O(5)	Fe(2)	N(9)	90.6 (2)
O(1)	Fe(1)	N(4)	88.20 (8)	N(6)	Fe(2)	N(7)	76.29 (9)
O(2)	Fe(1)	O(4)	97.1 (2)	N(6)	Fe(2)	N(9)	78.7 (1)
O(2)	Fe(1)	N(1)	166.64 (8)	N(7)	Fe(2)	N(9)	98.6 (2)
O(2)	Fe(1)	N(2)	95.45 (9)	Fe(1)	O(1)	Fe(2)	115.17 (8)
O(2)	Fe(1)	N(4)	93.1 (2)	O(3)	Fe(2)	N(4)	86.2 (1)
O(4)	Fe(1)	N(1)	91.35 (9)	O(3)	Fe(2)	N(9)	172.0 (1)
O(4)	Fe(1)	N(2)	82.47 (9)	O(5)	Fe(2)	N(6)	168.80 (9)
O(4)	Fe(1)	N(4)	169.8 (2)	Fe(1)	O(1)	C(1)	124.4 (1)
N(1)	Fe(1)	N(2)	75.33 (8)	Fe(2)	O(1)	C(1)	120.4 (1)
N(1)	Fe(1)	N(4)	78.46 (9)	Fe(1)	O(2)	C(30)	129.3 (2)
N(2)	Fe(1)	N(4)	95.34 (9)	Fe(2)	O(3)	C(30)	138.5 (2)
O(1)	Fe(2)	O(3)	86.30 (8)	Fe(1)	O(4)	C(37)	139.5 (2)
O(1)	Fe(2)	O(5)	96.70 (9)	Fe(2)	O(5)	C(37)	127.4 (2)
O(1)	Fe(2)	N(6)	86.13 (7)	Fe(1)	N(1)	C(8)	109.0 (2)
O(1)	Fe(2)	N(7)	160.0 (1)	Fe(1)	N(1)	C(10)	106.9 (2)
O(1)	Fe(2)	N(9)	87.08 (8)	Fe(1)	N(1)	C(15)	109.5 (2)

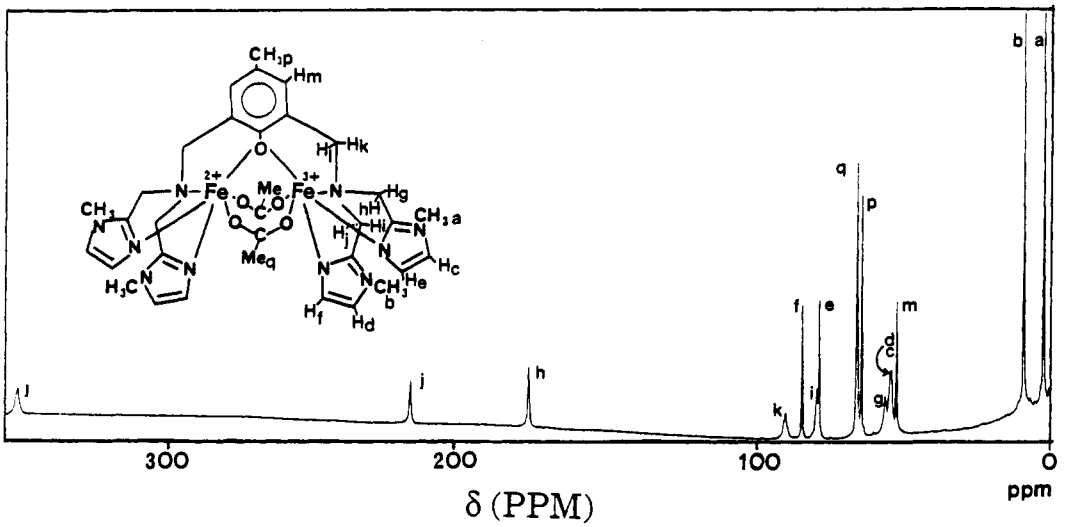

Figure 1. Room-temperature ^1H NMR spectrum of $[Fe^{II}Fe^{III}(bimp)(O_2CCH_3)_2](ClO_4)_2$ in CD_3CN.

$(bimp)(\mu\text{-}O_2CR)_2](X)_2$ (R = CH_3, C_2H_5, or C_6H_5 and X = ClO_4^-, BF_4^-, or $B(C_6H_5)_4^-$) are readily prepared by adding 2 equiv of an appropriate Fe^{II} salt to a methanolic solution containing Hbimp and sodium carboxylate, in a manner similar to that used to prepare $[Mn^{II}Mn^{III}(bimp)(\mu\text{-}O_2CCH_3)_2](ClO_4)_2$.[82] Similarly, $[Fe^{II}Fe^{III}(bimp)(\mu\text{-}O_2CR)_2]^{2+}$ complexes can be prepared by a sequential metalation procedure resembling that reported previously by us[83] and by Borovik and Que[73c] and by Suzuki et al.[74a] to prepare heterobimetallic complexes.

^1H NMR Studies. ^1H NMR spectroscopy has been established[73a,84,85] as a useful probe of the structural and magnetic properties of non-heme iron proteins. NMR has been used recently

(82) Buchanan, R. M.; Oberhausen, K. J.; Richardson, J. F. *Inorg. Chem.* **1988**, *27*, 971–973.

(83) Buchanan, R. M.; Mashuta, M. S.; Richardson, J. F.; Webb, R. J.; Oberhausen, K. J.; Nanny, M. A.; Hendrickson, D. N. *Inorg. Chem.* **1990**, *29*, 1299–1302.

(84) Maroney, M. J.; Lauffer, R. B.; Que, L., Jr.; Kurtz, D. M., Jr. *J. Am. Chem. Soc.* **1984**, *106*, 6445–6446.

(85) Wu, F.-J.; Kurtz, D. M., Jr. *J. Am. Chem. Soc.* **1989**, *111*, 6563–6572.

to characterize the structures of several $Fe^{II}Fe^{III}$ complexes in solution. In our studies, compounds **4**, **5**, and **9** were found to be strongly paramagnetic in acetonitrile solutions and exhibit well-resolved ^1H NMR spectra. Figure 1 shows the ^1H NMR spectrum of compound **4** in acetonitrile solution. The isotropically shifted signals span a range of about 350 ppm in all three complexes, consistent with results reported for other phenolate bridged $Fe^{II}Fe^{III}$ compounds. The NMR spectrum of complex **10**, on the other hand, displays only a few broad signals between 0 and 90 ppm, consistent with slow spin–lattice relaxation expected for a high-spin Fe^{III} complex. The large span of chemical shifts for the mixed-valence complexes suggest that the exchange interaction between the iron centers is weak. No noticeable changes were obtained in the spectra of **4** and **5** run at different (5–10 mmol) concentrations of the cations nor were there significant differences noted for different counterions. The narrow line widths of the signals (Figure 1) are consistent with the presence of a high-spin octahedral Fe^{II} center, which has a short T_{1e} relaxation time.[86] The spectrum of **5** resembles those of $[Fe^{II}Fe^{III}(bpmp)(\mu\text{-}OPr)_2]^{2+}$ [73c] and $[Fe^{II}Fe^{III}(hxta)(\mu\text{-}OPr)_2]^-$.[62]

Only 15 sharp well-resolved signals are observed in the spectrum of compound **4**. Twenty-nine signals would be expected for a static $Fe^{II}Fe^{III}$ configuration. The spectrum of **9** is complicated in the 0–15 ppm chemical shift range due to the presence of the tetraphenylborate counterions but overall it resembles the spectrum of compounds **4** and **5**. Therefore, it appears that intramolecular electron transfer in these complexes is fast on the NMR time scale. An alternative explanation of the signal averaging would involve rapid intermolecular electron transfer due to clustering of the cations at the concentrations used. Unfortunately, the signal-to-noise ratios for these spectra do not permit wide enough variation in concentrations to discriminate between these two possibilities. Signal assignments for compounds **4** and **5** are listed in the Experimental Section and were made based on relative line widths, integration intensity data, and T_1 measurements. For compound **4**, two resonances are observed at 7.05 and 13.38 ppm and are assigned to methyl substituents of two inequivalent imidazole rings. The methyl protons of the bridging acetate groups appear as a singlet at 67.26 ppm. The methyl signal associated with the phenol ring appears at 65.68 ppm. Four inequivalent imidazole ring protons are observed in the spectrum of **4**. The signals at 55.85 and 56.47 ppm are assigned to the 5-position protons of inequivalent rings while the 4-position protons are shifted further downfield to 79.61 and 85.21 ppm. Two inequivalent methylene protons are also observed at different chemical shift positions due to their proximity to the paramagnetic centers. The methylene protons directed away from the metal centers are shifted downfield to a lesser extent. The signals at 57.94 and 174.76 ppm are assigned to one set of methylene protons attached to two bmima units, while the signals at 80.40 and 214.0 ppm are assigned to the other set of methylene protons. The benzylic CH_2 signals are shifted further downfield and are slightly broader. The resonance at 342.05 ppm is assigned to the benzylic methylene proton directed toward the iron centers, whereas the signal at 90.72 ppm is assigned to the remaining benzylic protons that are directed away from the iron centers. Finally, the meta protons of the phenol ring are observed at 54.18 ppm. Analysis of spectra of compounds **4** and **5** reveals only slight differences in chemical shifts of individual nuclei. In particular, the methyl signal of the bridging proprionate groups appear at 20.35 ppm. The methylene protons are inequivalent and appear at 66.10 and 40.62 ppm. Similar diastereotopic pairs of propionate methylene signals are observed in the ^1H NMR spectrum of $[Fe^{II}Fe^{III}(bpmp)(\mu\text{-}OPr)_2]^{2+}$.[73b,c]

UV–Vis–Near-IR Electronic Absorption Spectra. The electronic absorption spectrum of **4** (figure available in supplementary material) displays features which are observed in the spectra of all of the $Fe^{II}Fe^{III}$–bimp complexes. In general, the electronic spectra of complexes **4**–**9** in acetonitrile exhibit broad absorption bands near 1300 nm (ϵ = 180–200 M^{-1} cm^{-1}) in the near-IR region. Diferrous[59,73c] and diferric[56,58] complexes do not show strong near-IR bands at wavelengths greater than 1100 nm; therefore the band near 1330 nm is assignable to an intervalence-transfer (IT) charge-transfer transition. This IT band is absent in the heterobimetallic complex $[Fe^{III}Zn^{II}(bimp)(\mu\text{-}OAc)_2]^{2+}$.[83] Similar IT bands have been reported for mixed-valence binuclear iron complexes of hxta,[73a] bpmp,[74a] and bzim.[74b] Borovik et al.[73a] have reported two IT-bands at 840 and 1275 nm for $Fe^{II}Fe^{III}(hxta)(OPr)_2$. One IT-band was observed in the near-infrared region at 1340 nm for $[Fe^{II}Fe^{III}(bpmp)(OPr)_2]^{2+}$. Suzuki et al.[74b] reported observing two IT bands near 1410 and 1350 nm for a series of $Fe^{II}Fe^{III}$(bzim) complexes.

The electronic spectra also reveal the presence of two bands at 960 and 375 nm in compound **4**. On the basis of its intensity and location, the band at 960 nm is tentatively assigned to the $^5T_2 \rightarrow {}^5E$ transitions expected for an octahedrally coordinated high-spin ferrous center. The extinction coefficient for the 375-nm band suggests that it is largely charge transfer in character. All of the mixed-valence bimp complexes display a strong absorption near 523 nm which can be assigned to a phenolate-to-Fe^{III} charge-transfer transition. These bands are due to charge-transfer transitions from filled $p\pi$ orbitals of the bridging phenolate oxygen atom to the half-filled $d\pi^*$ orbital of the Fe(III) metal center. Similar phenolate-to-Fe(III) charge-transfer transitions are observed at 470, 554, and 570 nm for $Fe^{II}Fe^{III}$ complexes of hxta, bpmp, and bzim, respectively. In the near-UV region each diiron bimp complex displays an intense absorption at 306 nm attributable to imidazole and phenol $\pi \rightarrow \pi^*$ transitions.

For semi-met-HrN_3, Sanders-Loehr et al.[87] reported observing two near-IR bands at 910 (ϵ = 10 M^{-1} cm^{-1}) and 1190 nm (ϵ = 16 M^{-1} cm^{-1}). The broad band at 1190 nm in the protein was attributed to a Fe^{II} ligand-field excitation enhanced by partial electron delocalization of the mixed-valence excited state. Thus, the lowest energy near-IR band was assigned to an intervalent charge-transfer transition. The higher energy near-IR band at 910 nm observed in the protein was assigned to the $^6A_1 \rightarrow {}^4T_1(^4G)$ ligand field transition expected for an octahedrally coordinated high-spin ferric ion.

Cyclic Voltammetry. The electrochemical properties of several $[Fe^{II}Fe^{III}(bimp)(O_2CR)_2](X_2)$ complexes have been investigated by cyclic voltammetry, since the redox properties play a critical role in the formation and stabilization of such mixed-valence complexes. Two single, quasireversible, one-electron processes are observed at –0.18 V and +0.477 V vs Ag/AgCl for the perchlorate salts in acetonitrile with 0.1 M $(Bu_4^nN)(ClO_4)$ electrolyte at a platinum electrode (figure available in supplementary material). The tetraphenylborate and tetrafluoroborate salts display slight shifts in the redox potentials with their waves occurring at –0.20 V and +0.48 V vs the Ag/AgCl reference electrode. The two quasireversible one-electron waves correspond to the $Fe^{II}Fe^{II}/Fe^{II}Fe^{III}$ and $Fe^{II}Fe^{III}/Fe^{III}Fe^{III}$ couples, respectively. All of the redox couples display peak-to-peak separations close to 80 mV and $E_{1/2}$ values that are independent of scan rate from 20 to 200 mV/s, with each couple having i_{p_c}/i_{p_a} ratios close to unity.[88]

From the separation of the two redox potentials in each cyclic voltammogram and the equation, $E^\circ_2 - E^\circ_1 = (RT/F) \ln K$, we have been able to determine the thermodynamic stability of the mixed complexes as gauged by the comproportionation constants (K_{com}) of the complexes. The values of K_{com} obtained for complexes **4**, **5**, and **9** are 3.10×10^{11}, 3.10×10^{11} M^{-1}, and 6.12×10^{11}, respectively, indicating that the mixed-valence diiron complexes of $bimp^-$ are highly stabilized.

Suzuki et al.[74] recently reported electrochemical data for several benzimidazole and polypyridyl $Fe^{II}Fe^{III}$ mixed-valence complexes in acetonitrile. Two reversible redox waves were observed at –0.08

(86) Bertini, I.; Luchinat, C. *NMR of Paramagnetic Molecules in Biological Systems*; Benjamin/Cummings: Menlo Park, CA, 1986.

(87) Sanders-Loehr, J.; Loehr, T. M.; Mauk, A. G.; Gray, H. B. *J. Am. Chem. Soc.* **1980**, *102*, 6992–6996.

(88) Bard, A. J.; Faulkner, L. R. *Electrochemical Methods*; John Wiley & Sons: New York, 1980.

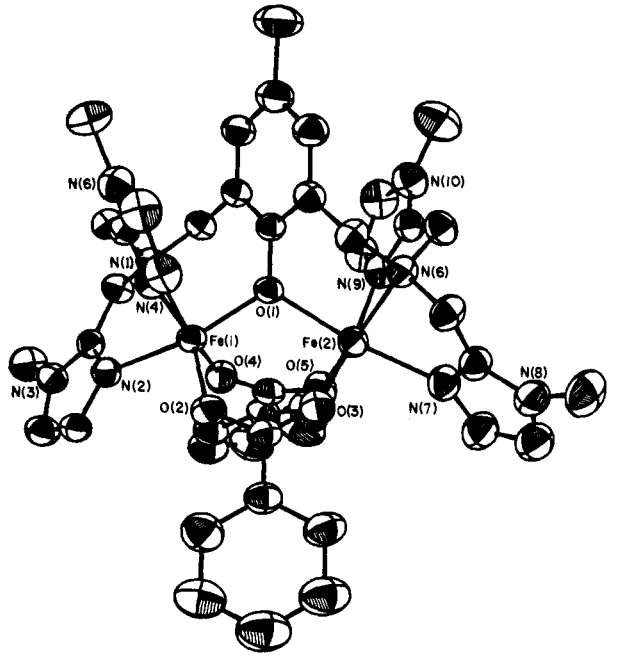

Figure 2. ORTEP plot of the cation in $[Fe^{II}Fe^{III}(bimp)(O_2CPh)_2](BPh_4)_2 \cdot {}^3/_2CH_3CN$.

and +0.60 V vs Ag/AgCl for $[Fe_2(bzim)(O_2CCH_3)_2]^{n+}$. The cyclic voltammogram of the di-μ-benzoate benzimidazole complex exhibited two redox waves at +0.04 and +0.70 V vs Ag/AgCl. Greater anodic potentials were observed for the polypyridyl complexes. Suzuki reported redox couples at +0.01 and +0.72 vs Ag/AgCl for $[Fe_2(bpmp)(OAc)_2]^{n+}$. The analogous benzoate bridged pyridyl complex exhibits two waves at +0.09 and +0.77 V vs Ag/AgCl. In addition, Que has reported the redox potentials of +0.04 and +0.73 V vs Ag/AgCl for $[Fe_2(bpmp)(OPr)_2]^{n+}$.[73c] The voltammograms of the mixed-valence polypyridyl and benzimidazole complexes all show redox processes 100–300 mV more positive than those observed for the $Fe^{II}Fe^{III}$(bimp) complexes. Interestingly, the difference between the two redox potentials for each complex remains constant at ~600 mV throughout all of the bzim, bpmp, and bimp complexes.

X-ray Structure of $[Fe^{II}Fe^{III}(bimp)(\mu\text{-}O_2CPh)_2](BPh_4)_2 \cdot 1.5CH_3CN$ (9). The structure of complex **9** confirms the mixed-valence nature of the dinuclear complex by displaying distinct Fe^{II} and Fe^{III} coordination environments. The complex crystallizes in the triclinic space group $P\bar{1}$ and consists of two distinct cationic units and four $B(C_6H_5)_4^-$ counterions per unit cell.

Each unit cell contains 1.5 acetonitrile solvate molecules. An ORTEP view of the mixed valence cation is shown in Figure 2. A packing diagram is available in the supplementary material and illustrates the arrangement of cations and anions, as well as the positions of the acetonitrile solvate molecules. The arrangement of the cations and anions clearly forms a pocket near the cluster and channels oriented along the *c* axis of the crystal. The half occupancy acetonitrile molecule occupies a position in the center of the pocket while the full occupancy solvate molecule occupies a position nearer to the cation and is closer to the Fe^{II} cation. The tetraphenylborate counterions are not symmetrically distributed about the cation. They are closer to the Fe^{II} than the Fe^{III} ion. Asymmetry of the anion packing around a mixed-valence cation has been observed in other complexes.[89-91] In the case of several biferrocenium salts the asymmetric positioning of anions about a mixed-valence cation has been shown[90,91] to valence trap the mixed-valence cation. Comparable asymmetry is observed in other mixed valence complexes and may be contributing to the valence trapping observed in $[Mn^{II}Mn^{III}(bimp)(\mu\text{-}O_2CCH_3)]^{2+}$.[82] In the present case, it is possible that the proximity of the anion to the Fe^{II} site as opposed to the Fe^{III} site is contributing to the observed valence *de*trapping (vide infra).

The coordination geometry about each iron center in **9** is octahedral. In Table II are given selected bond distances and angles. The iron ions are bridged by the phenolate oxygen atom of the $bimp^-$ ligand as well as by two benzoate groups. The Fe(1)–O(1)–Fe(2) bridging angle is 115.17 (8)°, which is slightly larger than the 113.1 (1)° reported[73c] for the $bpmp^-$ complex. The oxidation states of the iron centers in the cation of complex **9** are clearly differentiated by the significant differences in Fe–O bond lengths. The Fe(1)–O(1) bond length is 1.958 (1) Å which compares favorably with Fe^{III}–O(phenolate) bonds in other complexes such as $[Fe_2(bpmp)(\mu\text{-}O_2CCH_2CH_3)]^{2+}$ (1.943 (2) Å)[73c] and $[Fe^{III}Zn^{II}(bpmp)(\mu\text{-}O_2CCH_2CH_3)_2]^{2+}$ (1.982 (3) Å). Significantly longer lengths are observed for Fe^{II}–O(phenolate) bonds. In compound **9**, the Fe(2)–O(1) bond length is 2.115 (1) Å, within the range of values reported[73c] for $[Fe_2(bpmp)(\mu\text{-}O_2CCH_2CH_3)_2]^{2+}$ (2.090 (2) Å) and the average length of 2.057 (1) Å in $[Fe_2(bpmp)(\mu\text{-}O_2CCH_2CH_3)_2]^+$. Variable Fe^{II}–O(benzoate) (2.076 and 2.129 Å) and Fe^{III}–O(benzoate) (2.017 and 1.944 Å) bond lengths are observed for complex **9**. The shorter Fe(1)–O(2) (1.944 Å) and Fe(2)–O(5) (2.076 Å) lengths are associated with benzoate oxygen atoms that are trans to tertiary amine nitrogen atoms (N(1) and N(6)). Similar shortening of bridging carboxylate lengths are observed in other $Fe^{II}Fe^{III}$ complexes. The Fe(1)–O(2) length is unusually short for a bridging carboxylate oxygen atom. The overall expansion of the bond distances and angles associated with the phenolate bridge in **9** compared to $[Fe_2(bpmp)(\mu\text{-}O_2CCH_2CH_3)_2]^{2+}$ indicates that $bimp^-$ prefers a more open structure compared to the $bpmp^-$ ligand, which may be a factor responsible (in conjunction with other structural parameters) for the valence detrapping phenomena observed in the Fe_2(bimp) complexes.

In the dinuclear cation of **9**, each iron center is coordinated to a tertiary amine nitrogen atom and two imidazole groups, with one cis and the other trans to the phenolate bridge. The Fe–N(amine) bond lengths (Fe(1)–N(1) = 2.264 (2), Fe(2)–N(6) = 2.301 (2) Å) are significantly longer than the Fe–N(imidazole) lengths (Fe(1)–N(2) = 2.105 (2) Å, Fe(1)–N(4) = 2.088 (2) Å, Fe(2)–N(7) = 2.125 (3) Å, Fe(2)–N(9) = 2.123 (3) Å) and on an average are 0.080 and 0.106 Å longer than the corresponding Fe^{III} and Fe^{II} lengths reported[73c] for $[Fe_2(bpmp)(\mu\text{-}O_2CCH_2CH_3)_2]^{2+}$. Long Fe–N bond lengths are observed in N_3-metHr and other oxo-bridged model compounds, but these bonds are associated with nitrogen atoms trans to the μ-oxo bridge. The lengthening of the N(1) and N(6) bond lengths therefore must be due to the constraining nature of the $bimp^-$ ligand. As with $[Fe_2(bpmp)(\mu\text{-}O_2CCH_2CH_3)_2]^{2+}$, the N–Fe–N chelate angles are less than 90° (N(1)–Fe(1)–N(2) = 75.33 (8)°; N(1)–Fe(1)–N(4) = 78.46 (9)°; N(6)–Fe(2)–N(7) = 76.29 (9)°; N6–Fe(2)–N(9) = 78.7 (1)°). Other bond angles in the complex deviate significantly from those expected for octahedral geometry. The structural parameters of **9** suggest that the constraining nature of the $bimp^-$ ligand results in longer Fe–N(amine) bond lengths and shorter Fe–N(imidazole) bond lengths compared to the Fe–N lengths in $[Fe_2(bpmp)(\mu\text{-}O_2CCH_2CH_3)_2]^{2+}$. The shortening of the Fe–N(imidazole) lengths in complex **9** reflect the greater π contribution to the binding of imidazoles with iron compared to pyridine. Imidazole in general is thought to be a stronger π donor and acceptor ligand compared to pyridine. The greater strain in the coordination environment of the Fe_2(bimp) complex results in subtle but significant differences in $bimp^-$ and $bpmp^-$ as ligands. Moreover, the expanded coordination shell of the Fe^{III} site due to the constraints of the ligand could well affect the electron transfer properties of the complex (vide infra).

Magnetic Susceptibility. Variable-temperature magnetic susceptibility data were collected for two different samples of $[Fe^{II}Fe^{III}(bimp)(\mu\text{-}O_2CCH_3)_2](ClO_4)_2 \cdot 2H_2O$ (**4**) and for one sample of $[Fe^{II}Fe^{III}(bimp)(\mu\text{-}O_2CCH_3)_2](BF_4)_2 \cdot 2H_2O$ (**7**). As

(89) Geib, S. J.; Rheingold, A. L.; Dong, T.-Y.; Hendrickson, D. N. *J. Organomet. Chem.* **1986**, *312*, 241–248.
(90) Dong, T.-Y.; Hendrickson, D. N.; Pierpont, C. G.; Moore, M. F. *J. Am. Chem. Soc.* **1986**, *108*, 963–971.
(91) Webb, R. J.; Geib, S. J.; Staley, D. L.; Rheingold, A. L.; Hendrickson, D. N. *J. Am. Chem. Soc.* **1990**, *112*, 5031–5042.

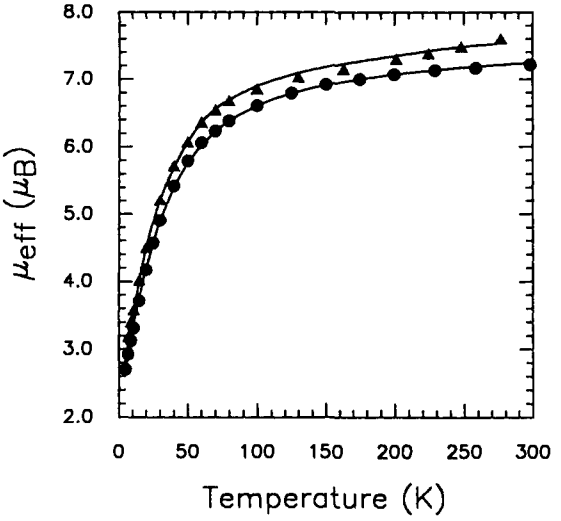

Figure 3. Plots of effective magnetic moment per molecule versus temperature for two different polycrystalline samples of $[Fe^{II}Fe^{III}(bimp)(O_2CCH_3)_2](ClO_4)_2 \cdot 2H_2O$ (**4**): △, sample 1; ○, sample 2. The solid lines result from a matrix-diagonalization least-squares fit of the data. See text for parameters.

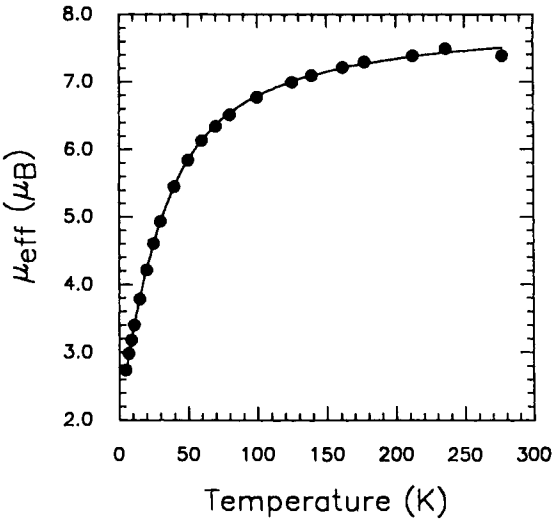

Figure 4. Plot of effective magnetic moment per molecule versus temperature for a polycrystalline sample of $[Fe^{II}Fe^{III}(bimp)(O_2CCH_3)_2](BF_4)_2 \cdot H_2O$ (**7**). The solid line results from a matrix-diagonalization least-squares fit of the data. See text for parameters.

can be seen in Figure 3, the shapes of the μ_{eff} versus temperature curves for the two different samples of the ClO_4^- salt are similar. Sample 1 has an effective magnetic moment per molecule, μ_{eff}, which steadily decreases from 7.60 μ_B at 280.0 K down to 6.85 μ_B at 100.0 K, whereupon there is a more rapid decrease to 2.77 μ_B at 4.50 K. Sample 2 has a value of μ_{eff} which starts at 7.21 μ_B at 298.3 K, decreases to 6.60 μ_B at 100.0 K, and then more rapidly decreases to 2.70 μ_B at 5.00 K. The chemical analyses for these two samples show that both samples are hydrates with compositions close to $[Fe^{II}Fe^{III}(bimp)(\mu\text{-}O_2CCH_3)_2](ClO_4)_2 \cdot 2H_2O$. The difference in μ_{eff} values for the two samples of **4** could be due to variable losses of H_2O hydrate molecules in the SQUID susceptometer. Preliminary fitting[72] of the data for sample 2 of the ClO_4^- salt to the theoretical susceptibility equation resulting from an isotropic magnetic exchange interaction characterized by $\hat{H} = -2J\hat{S}_1 \cdot \hat{S}_2$, where $S_1 = 2$ and $S_2 = {}^5/_2$, gave $J = -2.5$ cm^{-1} and $g = 1.9$. The five possible states for a binuclear $Fe^{II}Fe^{III}$ complex have total spins of $S = {}^1/_2, {}^3/_2, {}^5/_2, {}^7/_2$, and ${}^9/_2$. Since $|J|$ is small for complex **4**, it was realized that single-iron zero-field interactions and Zeeman interactions could be of comparable magnitude to the magnetic exchange interaction. Therefore, diagonalization of the full Hamiltonian matrix is needed.

The spin Hamiltonian for a binuclear $S_1 = 2, S_2 = {}^5/_2$ complex assuming an isotropic Zeeman interaction is given in eq 1. The

$$\hat{H} = \beta H_z(g_1 S_{z1} + g_2 S_{z2}) - 2J\hat{S}_1 \cdot S_2 + D_1[\hat{S}_{z1}^2 - {}^1/_3 S_1(S_1 + 1)] + D_2[\hat{S}_{z2}^2 - {}^1/_3 S_2(S_2 + 1)] \quad (1)$$

parameter D_1 gauges the axial single-ion, zero-field interaction on the Fe^{II} ion and D_2 the axial single-ion, zero-field interaction on the Fe^{III} ion. Rhombic single-ion, zero-field interactions were not included. The parameters g_1 and g_2 are the g factors for the Fe^{II} and Fe^{III} ions, respectively. It is important to note that it was also assumed that the single-ion, zero-field tensors on the two metal ions in the complex are collinear. While this is not necessarily the case, the available data do not warrant adding the three extra (angular) parameters necessary to handle any misalignment. With the present reasonably sophisticated model there are five parameters: g_1, g_2, J, D_1, and D_2; however, the g value for the Fe^{III} ion, i.e., g_2, should be equal to 2.00. A least-squares fitting computer program[92] was constructed, which for each setting of these four parameters diagonalized the 30 × 30 matrix resultant from eq 1. After each diagonalization, the energies (E_i) and magnetic moments ($\delta E_i/\delta H$) of each state were used to calculate the magnetization using eq 2. In eq 2, N is

$$M = N\sum_{i=1}^{n}(-\delta E_i/\delta H)\exp(-E_i/kT)/\sum_{i=1}^{n}\exp(-E_i/kT) \quad (2)$$

Avogadro's number and the summation runs over all states (i.e., all components of the above mentioned spin states). The molar paramagnetic susceptibility ($\chi_M = M/H$) is then easily evaluated as a function of temperature from the calculated magnetization. Since an octahedral Fe^{III} complex should have a small single-ion, zero-field interaction ($|D_2| < 0.1$ cm^{-1}),[43] it was decided to fix $D_2 = 0$ to give only three parameters: g_1, D_1, and J. The value of the temperature-independent paramagnetism (TIP) was held constant at 400 × 10^{-6} cgs per binuclear complex. It is important to note that Day et al.[20c] used a full matrix diagonalization treatment with the spin Hamiltonian in eq 1 to describe the mixed-valence center in uteroferrin. In their detailed study they accounted for saturation magnetization data measured at four magnetic fields, the EPR g values, and the magnetic Mössbauer parameters. Since our susceptibility studies were carried out on microcrystalline solids, we could not use the EPR g values from glass samples (vide supra). The EPR signals from our microcrystalline solids are too broad to give precise g values.

The data for the second sample of the ClO_4^- salt were fit to give $J = -3.4$ cm^{-1}, $D_1 = 0.63$ cm^{-1}, and $g_1 = 1.86$. It was necessary to include 0.33% by weight of a paramagnetic impurity (assumed to be a Fe^{III} monomeric analogue). The solid line shown in Figure 3 for the second sample data set represents this least-squares fit. A thorough examination of all parameter space showed that variations in g_1, D_1, D_2, or the amount of paramagnetic impurity affected the value of J by less than 10%.

The susceptibility data for sample 1 of the ClO_4^- salt complex **4** were also fit with D_2 held fixed at zero. This gave $J = -3.0$ cm^{-1}, $D_1(Fe^{II}) = 0.95$ cm^{-1}, and $g_1 = 1.94$ with 0.33% by weight of a monomeric Fe^{III} impurity. As can be seen by the second line in Figure 3, this fit is also good. The two data sets for samples 1 and 2 of complex **4** differ the most in the high temperature region. In fitting the two data sets this difference leads to the g_1 value changing. It was found that changing the g_1 value has little effect on the least-squares fitting value of J.

A plot of μ_{eff} for binuclear complex versus temperature is given in Figure 4 for a sample of $[Fe^{II}Fe^{III}(bimp)(\mu\text{-}O_2CCH_3)_2](BF_4)_2 \cdot H_2O$ (**7**). The value of μ_{eff} decreases from 7.38 μ_B at 277.2 K to 6.77 μ_B at 99.85 K, whereupon it decreases more rapidly to 2.74 μ_B at 5.00 K. These data were fit with $D_2 = 0$ to give $J = -3.7$ cm^{-1}, $D_1(Fe^{II}) = 0.53$ cm^{-1}, and $g_1 = 1.98$. These parameters are quite close to those found for sample 2 of the ClO_4^- salt. In

(92) Schmitt, E. A.; Hendrickson, D. N. Unpublished results.
(93) Cotton, F. A.; Gibson, J. F. *J. Chem. Soc. A* **1971**, 1696, and references therein.

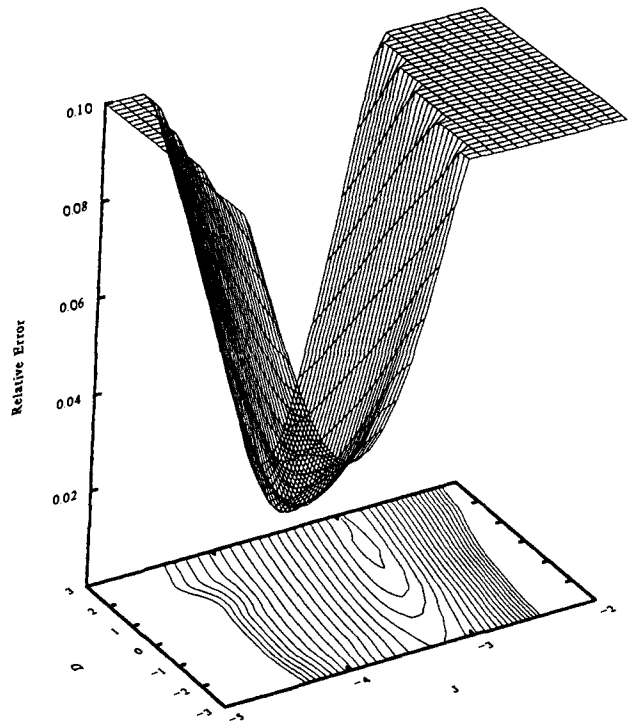

Figure 5. Contour plot of the error of fitting as a function of fitting parameters J and D_1 for the second sample of $[Fe^{II}Fe^{III}(bimp)(O_2CCH_3)_2](ClO_4)_2 \cdot 2H_2O$ (**4**).

Figure 7 it can be seen that the fit of the data for BF_4^- complex **7** is also good.

Even though the values of D_1 obtained from fitting the data for complexes **4** and **7** are reasonable, one caveat has to be raised. It is known[94] that a determination of zero-field interaction parameters with bulk susceptibility data does *not* give a very accurate evaluation of the D parameters. In Figure 5 is shown for the second sample data set of complex **4** a contour plot of the error of fitting as function of the two fitting parameters J and D_1. Similar plots were found for the other data sets. As can be seen in Figure 5, there is a reasonably good responsiveness to changing J. The value of J is well characterized as -3.4 cm^{-1}. However, there is a trough where D_1 can be varied from approximately $+3$ cm^{-1} to -2 cm^{-1} with little impact on the error of fitting the data. Figure 5 thus shows that D_1 is poorly defined by fitting the bulk susceptibility data. Furthermore, since it was assumed that the **D** tensors and **g** tensors are colinear on the Fe^{II} and Fe^{III} ions, it is expected that the value of D_1 is not known well. The magnitude of the magnetic exchange interactions present[73,74] in $Fe^{II}Fe^{III}$ complexes formed with the pyridyl-armed ($bpmp^-$) or benzimidazole-armed ligand analogues of $bimp^-$ have not been thoroughly characterized. Suzuki et al.[74] have only measured susceptibility data in the 80–300 K range. They concluded that very weak antiferromagnetic interactions are present in these binuclear $Fe^{II}Fe^{III}$ complexes.

The magnitude of the J value (~ -3 cm^{-1}) determined in this study for salts of $[Fe^{II}Fe^{III}(bimp)(\mu\text{-}O_2CCH_3)_2]^{2+}$ is intriguing. If, as seems reasonable, such a very weak antiferromagnetic interaction is present in the $Fe^{II}Fe^{III}$ forms of various μ-oxo proteins,[14] then this would help explain the sensitivity of the EPR signal to just what procedure was employed to prepare the $Fe^{II}Fe^{III}$ protein. A mixed-valence $Fe^{II}Fe^{III}$ complex with a weak exchange interaction should be very sensitive to its environment. A change in the counteranion, solvate molecule in the crystal, or the details of the conformation and configuration of protein structure about a vibronically active $Fe^{II}Fe^{III}$ center could affect its intramolecular electron-transfer rate.

(94) Carlin, R. L. *Magnetochemistry*; Springer-Verlag: New York, 1986; Chapter 2.

^{57}Fe Mössbauer Spectroscopy. Considerable Mössbauer data were collected for five of the $Fe^{II}Fe^{III}$(bimp) complexes. The figure in our previous communication[72] illustrates spectra obtained for sample 2 of $[Fe^{II}Fe^{III}(bimp)(\mu\text{-}O_2CCH_3)_2](ClO_4)_2 \cdot 2H_2O$ (**4**). It is clear that there is a temperature dependence in the spectrum. After careful examination of these spectra, it is easy to conclude that much of the temperature dependence must be associated with the mixed-valence cation converting from being valence trapped at low temperature to valence detrapped at the higher temperatures. One very good piece of evidence that this is occurring can be gleaned from the temperature dependence seen for the peak at a velocity of +1.7 mm/s in the 100 K spectrum. Based on the anticipated relative magnitudes of ΔE_Q for a high-spin Fe^{II} ion versus a high-spin Fe^{III} ion, this outermost resonance is no doubt the positive velocity component of the Fe^{II} doublet. It can be seen that, as the temperature of this complex **4** is increased from 100 to 150 and then to 250 K, the $\sim$+1.7 mm/s peak moves to a lower velocity position. The quadrupole splitting of a high-spin Fe^{II} doublet is expected to be somewhat temperature dependent; however, the magnitude of the observed temperature is only explicable in terms of a valence detrapping in the $Fe^{II}Fe^{III}$ complex. This same type of temperature dependence for the Mössbauer spectra of several $Fe_2^{III}Fe^{II}O$ complexes known to valence detrap on the timescale of the Mössbauer experiment is well documented.[95]

Each Mössbauer spectrum was fit with Lorentzian lineshapes. For a valence-trapped $Fe^{II}Fe^{III}$ complex two doublets (i.e., four Lorentzians with equal areas) were used to fit the spectrum. In the case of a valence-detrapped species, one doublet was used. For many spectra it was necessary to use a superposition (i.e., six Lorentzians) of valence-trapped and valence-detrapped signals. The parameters resulting from these fits are available in the supplementary material. However, because it is difficult to establish an unique fitting of a given spectrum with six Lorentzians and because it may be the case that these spectra need to be fit by a relaxation model, we do *not* discuss the fitting parameters for the complicated spectra.

It was not possible to fit the 100 K spectrum for complex **4** simply to two doublets of equal area as expected for a totally trapped $Fe^{II}Fe^{III}$ complex; it was necessary to employ three quadrupole-split doublets. One doublet has a splitting of ΔE_Q = 2.537 (8) mm/s and an isomer shift of δ = 0.881 (4) mm/s (vs iron foil); these parameters are characteristic of a high-spin Fe^{II} ion. A second doublet with an area fixed to be equal to that of the Fe^{II} doublet has parameters (ΔE_Q = 0.314 (3) mm/s and δ = 0.3997 (14) mm/s) which indicate a high-spin Fe^{III} ion. The third doublet with ΔE_Q = 1.065 (8) mm/s and δ = 0.567 (4) mm/s reflects some 46% of valence detrapped complexes. As the temperature is increased, the area percent for the detrapped doublet increases to a value of 60% at 350 K.

The Mössbauer spectra illustrated in Figure 6 for $[Fe^{II}Fe^{III}(bimp)(\mu\text{-}O_2CCH_3)_2](BF_4)_2 \cdot H_2O$ provide convincing evidence of the spectral analysis presented above for the ClO_4^- salt of this same cation. The BF_4^- salt converts from being totally valence trapped at 110 K to essentially completely detrapped at 290 K. The 110 K spectrum is well fit by two quadrupole-split doublets, each constrained to have the same area. The Fe^{III} doublet has ΔE_Q = 0.321 (3) mm/s and δ = 0.507 (2) mm/s. These values are close to those observed at 100 K for the Fe^{III} doublet in the ClO_4^- salt. However, the Fe^{II} doublet in the 110 K spectrum of

(95) (a) Jang, H. G.; Geib, S. J.; Kaneko, Y.; Nakano, M.; Sorai, M.; Rheingold, A. L.; Montez, B.; Hendrickson, D. N. *J. Am. Chem. Soc.* **1989**, *111*, 173–186. (b) Kaneko, Y.; Nakano, M.; Sorai, M.; Jang, H. G.; Hendrickson, D. N. *Inorg. Chem.* **1989**, *28*, 1067–1073. (c) Oh, S. M.; Wilson, S. R.; Hendrickson, D. N.; Woehler, S. E.; Wittebort, R. J.; Inniss, D.; Strouse, C. E. *J. Am. Chem. Soc.* **1987**, *109*, 1073–1090. (d) Woehler, S. E.; Wittebort, R. J.; Oh, S. M.; Kambara, T.; Hendrickson, D. N.; Inniss, D.; Strouse, C. E. *J. Am. Chem. Soc.* **1987**, *109*, 1063–1067. (e) Woehler, S. E.; Wittebort, R. J.; Oh, S. M.; Hendrickson, D. N.; Inniss, D.; Strouse, C. E. *J. Am. Chem. Soc.* **1986**, *108*, 2938–2946. (f) Hendrickson, D. N.; Oh, S. M.; Dong, T.-Y.; Kambara, T.; Cohn, M. J.; Moore, M. F. *Comments Inorg. Chem.* **1985**, *4*, 329–349. (g) Sorai, M.; Kaji, K.; Hendrickson, D. N.; Oh, S. M. *J. Am. Chem. Soc.* **1986**, *108*, 702–708.

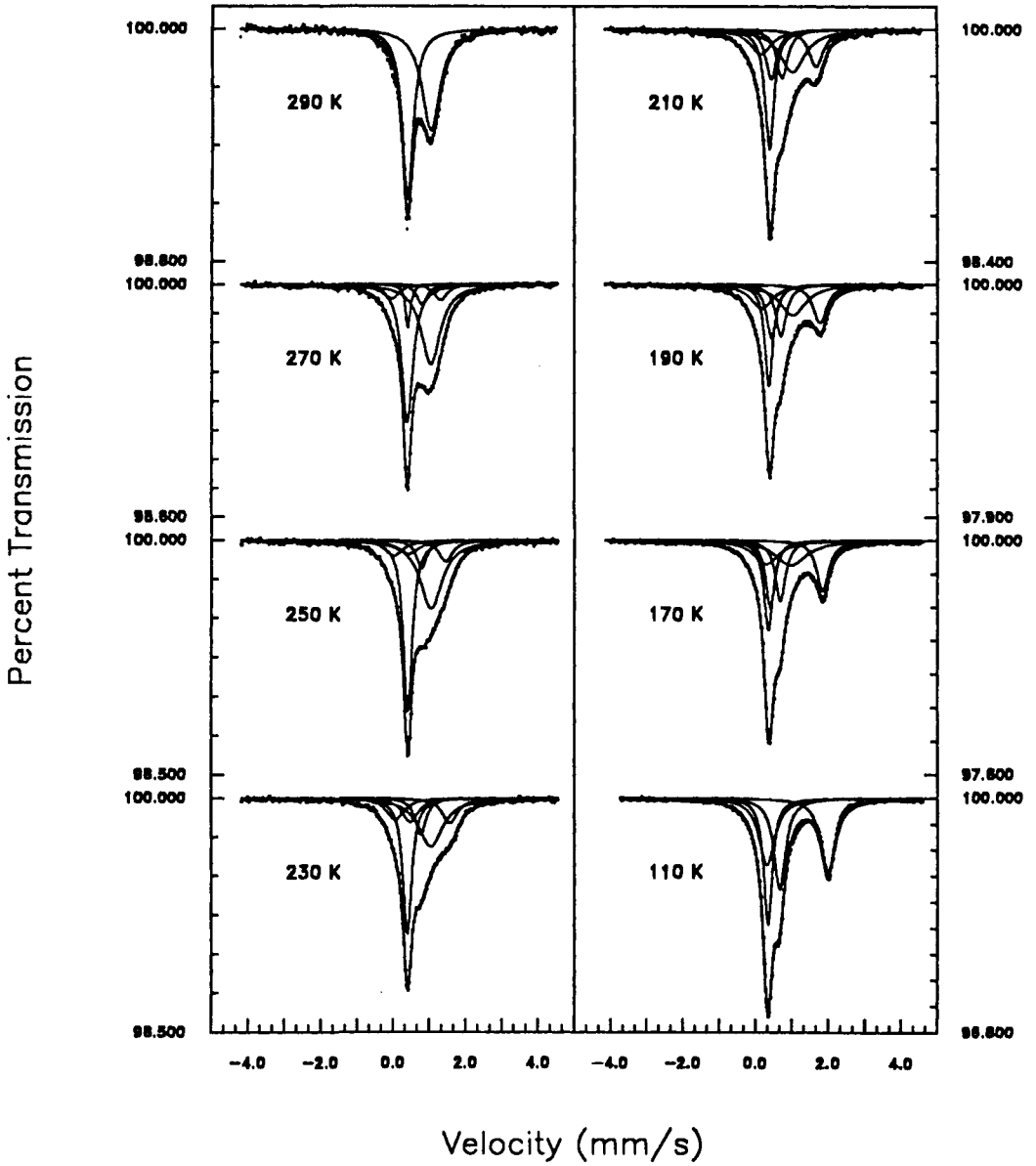

Figure 6. Variable-temperature ^{57}Fe Mössbauer spectra for a polycrystalline sample of $[Fe^{II}Fe^{III}(bimp)(O_2CCH_3)_2](BF_4)_2 \cdot H_2O$ (7).

the BF_4^- salt has fitting parameters (ΔE_Q = 1.685 (9) mm/s and δ = 1.157 (5) mm/s) which are different than those for the Fe^{II} doublet in the 100 K spectrum of the ClO_4^- salt. The Fe^{II} ion in the $[Fe^{II}Fe^{III}(bimp)(\mu\text{-}O_2CCH_3)_2]^{2+}$ cation is apparently sensitive to the nature of the anion. An increase in the temperature of the BF_4^- complex **7** from 110 to 170 K leads to a change in the appearance of the spectrum. The spectrum run at 290 K can essentially be fit by only one doublet for a detrapped species (the two components have different line widths). This singlet doublet at 290 K is characterized by ΔE_Q = 0.645 (5) mm/s and δ = 0.712 (2) mm/s. These parameters are interesting for two reasons. First, they are close to the parameters found for the detrapped doublet in the 350 K spectrum of the ClO_4^- salt. Second, the isomer shift parameter for this valence detrapped signal is more positive than the δ values for the Fe^{II} and Fe^{III} doublets obtained at 270 K.

Mössbauer spectra were run for a polycrystalline sample of $[Fe^{II}Fe^{III}(bimp)(O_2CPh)_2](ClO_4)_2 \cdot 2H_2O$ (**6**). A figure showing the data is available in the supplementary material. From fitting of the data we conclude that the complex is converting from ~76% valence detrapped at 100 K to essentially 100% detrapped at 300 K. However, there is a new feature. For this complex the 270 and 300 K spectra clearly exhibit two equal-area doublets, both of which are characteristic of valence-detrapped complexes. This can be explained if there were two different crystallographic sites for $Fe^{II}Fe^{III}$ cations for complex **6**, and the cations on the two different sites were interconverting faster than the Mössbauer timescale. If the distinction between the two lattice sites was great enough, then two valence-detrapped doublets would be seen. A crystallographically characterized mixed-valence biferrocene complex has been reported[91] which has two different cations, each of which detrap at higher temperatures.

Mössbauer spectra collected for two samples of $[Fe^{II}Fe^{III}(bimp)(O_2CCH_3)_2](BPh_4)_2 \cdot x(CH_3CN)$ (**9**) clearly show the sensitivity of these complexes to small environmental factors such as the amount of solvate molecules present. Sample 1 analyzed to have $x \simeq 2$ and sample 2 to have $x \simeq 0$. Figures 7 and 8 show how sensitive the properties of complex **9** are to the solvate molecule composition. The 100 K spectrum (Figure 7) for the $x \simeq 0$ polycrystalline sample has the pleasing simple appearance of a trapped spectrum, with equal-area Fe^{II} and Fe^{III} doublets. Fitting this spectrum shows that there is also ~9.6% of a third doublet for detrapped species. In Figure 8 it can be seen that the 100 K spectrum for the $x \simeq 2$ polycrystalline sample exhibits more (~44%) of the third doublet for the detrapped species. Fitting of the 300 K spectrum for the $x \simeq 2$ sample indicates this sample converts to ~85% detrapped, whereas the $x \simeq 0$ sample only converts to ~56% detrapped by 300 K.

The Mössbauer data for the $Fe^{II}Fe^{III}$(bimp) complexes clearly demonstrate several points. First, at low temperatures these complexes tend to exhibit distinct Fe^{II} and Fe^{III} valences. Second,

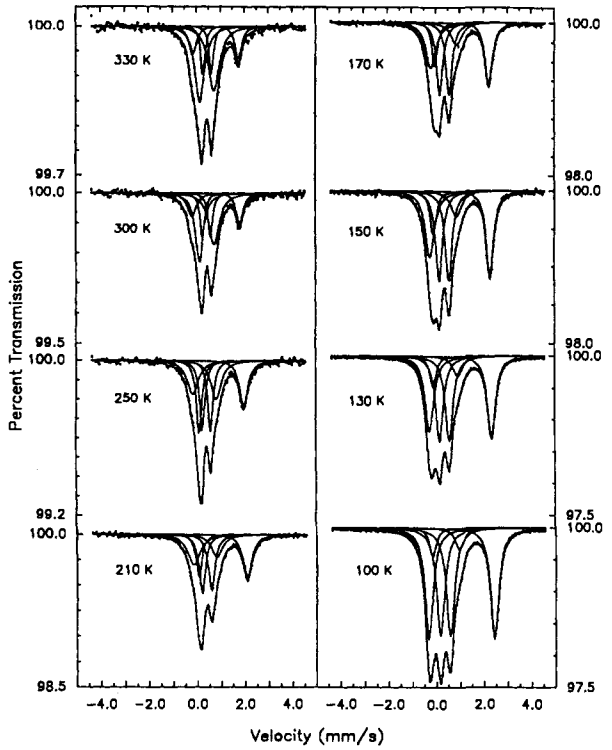

Figure 7. Variable-temperature ^{57}Fe Mössbauer spectra for a polycrystalline sample of $[Fe^{II}Fe^{III}(bimp)(O_2CC_6H_5)_2](BPh_4)_2$ (**9**). CH_3CN solvate molecules were pumped off this sample.

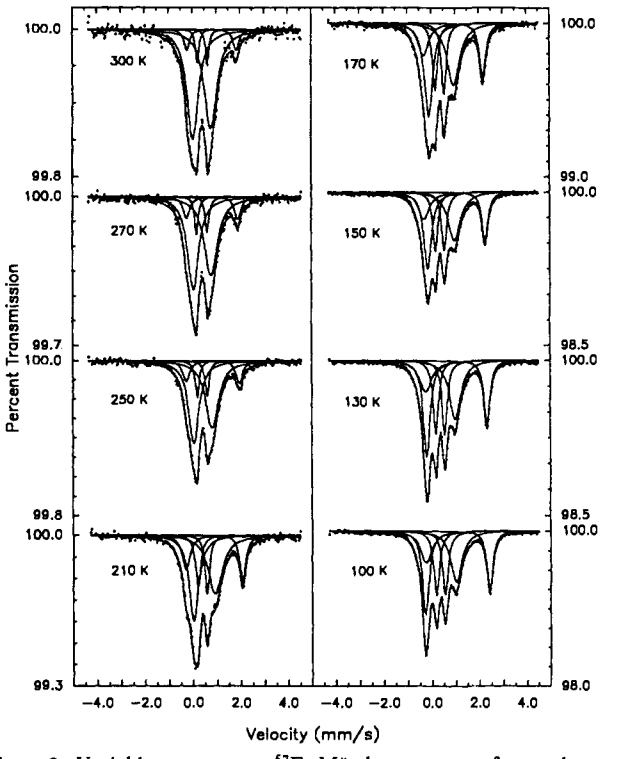

Figure 8. Variable-temperature ^{57}Fe Mössbauer spectra for a polycrystalline sample of $[Fe^{II}Fe^{III}(bimp)(O_2CC_6H_5)_2](BPh_4)_2 \cdot 2CH_3CN$ (**9**).

heating the samples leads to an increase in the number of molecules exhibiting rates of electron transfer which exceed the timescale of the ^{57}Fe Mössbauer experiment. Third, this temperature dependence depends on basic structural features such as the carboxylate bridge and anion as well as on subtle environmental features such as the solvate molecule composition. Changes in the carboxylate bridge and/or anion can obviously lead to a change in space group. However, a change in solvate molecule composition would likely in many cases *not* lead to a change in crystallographic

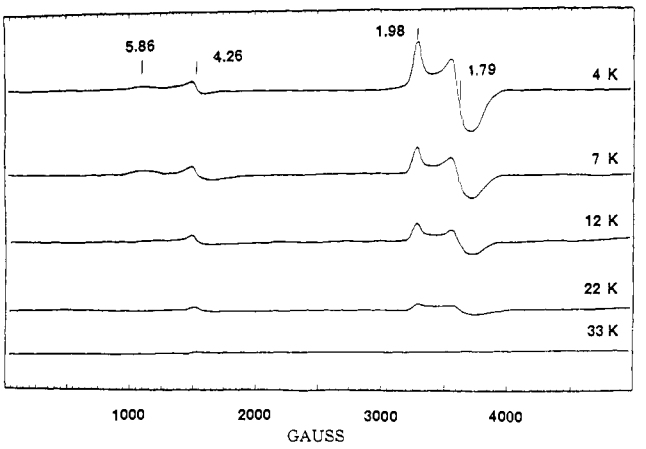

Figure 9. Variable-temperature frozen acetonitrile solution EPR spectra of compound **4**: microwave power, 5.0 mW; microwave frequency, 9.10 GHz; modulation amplitude, 2.5 G; modulation frequency, 100 kHz; gain, 6.3×10^1.

symmetry. Appreciable sensitivity to various subtle environmental factors is therefore established for these $Fe^{II}Fe^{III}$(bimp) complexes. A strong coupling of the electronic and vibrational coordinates leads to a sensitivity to the environment.[95,96] It is difficult to know why these $Fe^{II}Fe^{III}$(bimp) complexes exhibit valence detrapping, whereas the pyridine and benzimidazole analogues have not been reported to valence detrap at temperatures approaching room temperature. We have noted that there are differences in some of the bond lengths and angles between the $bimp^-$ complexes and the others.

EPR Spectroscopy. EPR spectroscopy has been used to probe the electronic structure of the mixed-valence forms of oxo-iron proteins.[1] The active sites of these proteins contain both high-spin $Fe^{II}(S = 2)$ and $Fe^{III}(S = {}^5/_2)$ ions that are coupled antiferromagnetically resulting in $S = {}^1/_2$ ground states. At temperatures near liquid He, the mixed valence proteins display unique axial and rhombic EPR spectra with g values less than 2.[1,3] These signals are sensitive to the nature of the bridge structure, solvent conditions, as well as the temperature at which the spectrum is measured. Similar $g < 2$ signals have been reported for several synthetic mixed valence complexes, such as $[Fe_2O(Me_3tacn)_2(\mu\text{-}OAc)_2]^{2+}$[55c] and $[Fe_2(O)(\mu\text{-}O_2CR)_2]^{2+}$ (L = bpmp,[74a] bzim[64] with R = C_6H_5 or C_2H_5). However, the spectra for several of the model complexes are very broad and do not display the unique axial or rhombic shapes observed for the oxo-iron proteins.

We reported earlier[72] that the EPR properties of the $[Fe^{II}Fe^{III}(bimp)(\mu\text{-}O_2CR)_2]X_2$ complexes depend on R, X^-, and the state of the complexes. Complexes **4** and **5** display sharp EPR signals in frozen acetonitrile solutions near helium temperature; the signals disappear above 30 K (Figure 9). The axial shapes, average g values, and temperature dependence of the signals are strikingly similar to the EPR spectrum reported for $(semimet)_o$ Hr (g = 1.95 and 1.72). The shape of the frozen solution spectrum of compound **8** is slightly different (Figure 10). The high field signal is split giving three g values (1.97, 1.79, and 1.72), resembling the spectra observed for reduced purple acid phosphatase (1.96, 1.73, and 1.56),[20] $(semimet)_r$ Hr (1.96, 1.88, 1.66),[1] and the mixed-valence form of methane monooxygenase (1.94, 1.86, and 1.75).[35] The origin of the splitting of the high field signal

(96) (a) Dong, T.-Y.; Cohn, M. J.; Hendrickson, D. N.; Pierpont, C. G. *J. Am. Chem. Soc.* **1985**, *107*, 4777–4778. (b) Cohn, M. J.; Dong, T.-Y.; Hendrickson, D. N.; Geib, S. J.; Rheingold, A. L. *J. Chem. Soc., Chem. Commun.* **1985**, 1095–1097. (c) Dong, T.-Y.; Hendrickson, D. N.; Iwai, K.; Cohn, M. J.; Rheingold, A. L.; Sano, H.; Motoyama, I.; Nakashima, S. *J. Am. Chem. Soc.* **1985**, *107*, 7996–8008. (d) Moore, M. F.; Wilson, S. R.; Cohn, M. J.; Dong, T.-Y.; Mueller-Westerhoff, U. T.; Hendrickson, D. N. *Inorg. Chem.* **1985**, *24*, 4559–4565. (e) Dong, T.-Y.; Kambara, T.; Hendrickson, D. N. *J. Am. Chem. Soc.* **1986**, *108*, 4423–4432. (f) Dong, T.-Y.; Kambara, T.; Hendrickson, D. N. *J. Am. Chem. Soc.* **1986**, *108*, 5857–5865. (g) Sorai, M.; Nishimori, A.; Hendrickson, D. N.; Dong, T.-Y.; Cohn, M. J. *J. Am. Chem. Soc.* **1987**, *109*, 4266–4275. (h) Kambara, T.; Hendrickson, D. N.; Dong, T.-Y.; Cohn, M. J. *J. Chem. Phys.* **1987**, *86*, 2362–2374.

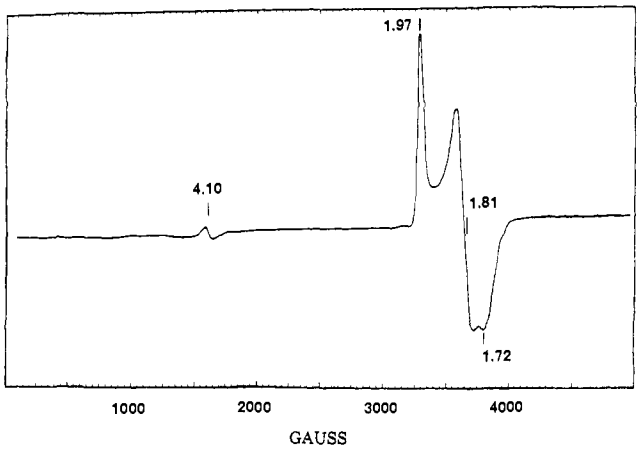

Figure 10. X-Band EPR spectrum of a frozen acetonitrile solution of compound **8** at 4.0 K: microwave power, 20 mW; microwave frequency, 9.10 GHz; modulation amplitude, 1.0 G; modulation frequency, 100 kHz; gain, 4×10^3.

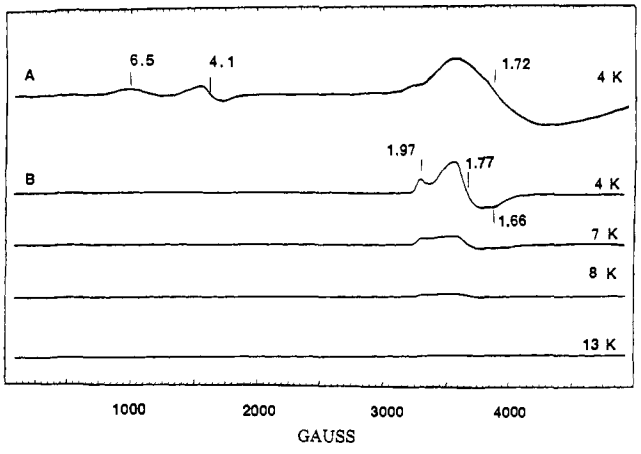

Figure 11. Polycrystalline powder EPR spectra of compounds **4** and **8** at various temperatures. Trace A is the powder spectrum of compound **4** at 4 K: microwave power, 20 mW; microwave frequency, 9.10 GHz; modulation amplitude, 1 G; modulation frequency, 100 kHz; gain, 1×10^3. Traces B–E are powder spectra of compound **8** at various frequencies: microwave power, 10 mW; microwave frequency, 9.10 GHz; modulation amplitude, 1 G; modulation frequency, 100 kHz; gain, 4×10^2.

is not clear at the present time; however a rhombic effective **g** tensor is expected in spin-coupled Fe^{II}–Fe^{III} complexes if the Fe^{II} ion has low symmetry. In fact, metathesis of the ClO_4^- counterions of compound **5** using $NaBPh_4$ results in a sample that displays a frozen acetonitrile EPR spectrum identical to the spectrum observed for compound **8**. In the polycrystalline phase, compounds **4** and **5** show broad EPR spectra with $g_{ave} = 1.7$ near 4 K, while compound **8** displays a more resolved spectrum with g values of 1.97, 1.77, and 1.66 (Figure 11). Broadening of the powder spectra suggests the presence of rapid spin–lattice relaxation. The better resolution of the spectrum of compound **8** indicates that BPh_4^- counterions provide greater magnetic dilution compared to the smaller ClO_4^- ions. Interestingly, similar broad spectra ($g_{ave} = 1.6$–1.7) are observed for compounds **4**, **5**, and **8** in frozen acetonitrile/toluene solutions.

The frozen acetonitrile solution spectra of compounds **7** and **9** are different from those discussed earlier. They resemble the spectra reported for the phosphate and arsenate complexes of reduced uteroferrin.[20c] The $g < 2$ signals are not observed at temperatures above 15 K and are extremely broad ($g = 1.5$–1.6) at 4 K. This may indicate that there is an increase in the effective g strain for the complexes resulting from a decrease in exchange coupling; where J and D are more comparable. As with the phosphate complex of uteroferrin, an increase in the anisotropy of the **g** tensor would cause broadening of the EPR spectrum, and if J is small, the signal would be difficult to detect at temperatures above 4 K.

In all of the solution spectra and in some of the solid-state spectra, a signal is observed near $g = 4.3$ which is attributed to the presence of a high-spin mononuclear Fe^{III} impurity. A similar signal is observed for the mononuclear Fe^{III}(bimp) complex **10** used to prepare the $Fe^{II}Fe^{III}$ complexes following method **2** as well as the heterobinuclear $Fe^{III}Zn^{II}$ complexes reported elsewhere.[75] In fact, mononuclear forms of the $bimp^-$ ligand have been prepared using other metal ions, suggesting that metalation of the phenol containing a polypodal ligands[74a,75,82] occurs in sequential metalation steps.

Broad signals between $g = 5$ and $g = 7$ also are observed in the spectra of several of the complexes which display a temperature dependence similar to the $g < 2$ signals. These signals may be due to transitions involving the $S = {}^3/_2$ lowest energy excited state. Since J is known to be small for compounds **4** and **7** and the single ion zero-field interaction for the Fe^{II} ion (D_1) is comparable in magnitude ($D_1 \approx J$) the $S = {}^1/_2$ and $S = {}^3/_2$ Kramers doublets of the $S = {}^3/_2$ state are expected to be close in energy to the $S = {}^1/_2$ ground state, as we observed in a series of $Mn^{II}Mn^{III}$ complexes having $S = {}^5/_2$ and $S = 2$ ion configurations.[82,97] More detailed variable temperature studies are required before these transitions can be definitively assigned.

Concluding Comments

Considerable data have been presented to show that the $[Fe^{II}Fe^{III}(bimp)(\mu\text{-}O_2CR)_2]X_2$ complexes are good model complexes for the $Fe^{II}Fe^{III}$ mixed-valence forms of iron–oxo proteins such as hemerythrin, ribonucleotide reductase, purple acid phosphatase, uteroferrin, and methane monooxygenase. Compared to other binuclearing ligands (bpmp and bzim) which have been used to prepare μ-phenoxo-bridged $Fe^{II}Fe^{III}$ model complexes, the imidazole arms on the $bimp^-$ ligand are better mimics of the ligands present at the protein sites. The two one-electron redox waves observed for the $Fe^{II}Fe^{III}$(bimp) complexes were found at potentials 100–300 mV more negative than the corresponding waves for the bpmp and bzim complexes. This is important to note for the functioning of the above proteins varies from reversible O_2 binding to O_2 activation to nucleotide reduction.

Relative to iron–oxo proteins two main lessons have been learned from the data on the $Fe^{II}Fe^{III}$(bimp) complexes. First, the basic nature of the electronic structure of the μ-phenoxo-bis(μ-carboxylato)$Fe^{II}Fe^{III}$ has been characterized. The 295 K X-ray structure of $[Fe^{II}Fe^{III}(bimp)(\mu\text{-}O_2CPh)_2](BPh_4)_2 \cdot {}^3/_2CH_3CN$ shows a trapped valence (Fe^{II} and Fe^{III} ions) electronic structure. There is only a very weak antiferromagnetic ($J \simeq -3.0\ cm^{-1}$) interaction between the Fe^{II} and Fe^{III} ions. Single-ion, zero-field (and Zeeman) interactions are of the same magnitude as the HDVV exchange interaction. It is somewhat surprising that, in spite of the very weak spin coupling, the $Fe^{II}Fe^{III}$(bimp) complexes have been shown by Mössbauer spectroscopy to valence detrap at temperatures near to room temperature. At temperatures below ~100 K the Fe^{II} and Fe^{III} valences are trapped. In summary, the first lesson is that the electronic structure of the $Fe^{II}Fe^{III}$(bimp) is quite *vibronic*. Because so many electronic states are nearly energetically degenerate, certain vibrational coordinates strongly couple to the electronic coordinates involved in the electron transfer.

The second lesson learned from the $Fe^{II}Fe^{III}$(bimp) complexes is that they are quite responsive to their environments. A change in the counteranion or even the solvate molecule can dramatically affect the rate at which these mixed-valence complexes interconvert between their two vibronic states $Fe_A^{II}Fe_B^{III}$ and $Fe_A^{III}Fe_B^{II}$. This sensitivity to environment is a direct consequence of the very vibronic nature of the $Fe^{II}Fe^{III}$(bimp) center. There are one or more relatively large amplitude vibrational motions which occur as the complex interconverts between the $Fe_A^{II}Fe_B^{III}$ and $Fe_A^{III}Fe_B^{II}$

(97) Diril, H.; Chang, H.-R.; Nilges, M. J.; Zhang, X.; Potenza, J. A.; Schugar, H. J.; Isied, S. S.; Hendrickson, D. N. *J. Am. Chem. Soc.* **1989**, *111*, 5102–5114, and references therein.

states. If there are appreciable intermolecular interactions present between cations/anions/solvate molecules in the crystal of a $Fe^{II}Fe^{III}$(bimp) complex, then these interactions will tend to valence trap the complex. The complex will not have enough thermal energy to make an interconversion, overcoming interactions with neighboring molecules in the crystal. The sensitivity of this phenomenon is highlighted by the solvate molecule dependence observed for the $Fe^{II}Fe^{III}$(bimp) complexes. A solvate molecule is generally sitting in a crystal site near to the $Fe^{II}Fe^{III}$ cation. There are perhaps only weak van der Waals interactions; however they can be strong enough to valence trap the complex. As the crystal temperature is increased, the solvate–complex interaction weakens and in many cases the solvate molecules convert from being static to being dynamic. The $Fe^{II}Fe^{III}$(bimp) complex now finds itself in a more "pliable" environment in which it can make its large-amplitude motion necessary for the electron transfer.

The environmental sensitivity seen for the $Fe^{II}Fe^{III}$(bimp) complexes has implications for the iron–oxo $Fe^{II}Fe^{III}$ protein sites. These sites are likely very much influenced by the protein structure. Conformational changes of the protein, triggered off by substrate binding, docking with another protein, or configurational changes in the membrane to which the protein is attached, can have pronounced effects on the rate of electron transfer in the $Fe^{II}Fe^{III}$ protein site. This "environmental" sensitivity also provides an explanation for why the EPR signals for these $Fe^{II}Fe^{III}$ proteins are sensitive to whether the $Fe^{II}Fe^{III}$ protein form is prepared by either oxidizing the Fe_2^{II} protein or reducing the Fe_2^{III} protein.[43] The manner in which frozen solution protein sample is prepared for EPR studies, by slow or rapid cooling for example, could influence the appearance of the EPR signal.

Acknowledgment. This work was supported by the National Institutes of Health Grants HL13652 (D.N.H.) and GM45783, National Science Foundation Grant R11-8610671, and the Commonwealth of Kentucky through the Kentucky EPSCoR program (R.M.B.).

Supplementary Material Available: Tables of positional parameters, anisotropic thermal parameters, and hydrogen atom positional parameters and stereoplot of packing arrangement for $[Fe^{II}Fe^{III}(bimp)(O_2CPh)_2](BPh_4)_2 \cdot {}^3/_2CH_3CN$, table of Mössbauer spectra for $[Fe^{II}Fe^{III}(bimp)(O_2CCH_3)_2](ClO_4)_2 \cdot 2H_2O$, table of magnetic susceptibility for $[Fe^{II}Fe^{III}(bimp)(O_2CCH_3)_2](BF_4)_2$, figure of Mössbauer spectra for $[Fe^{II}Fe^{III}(bimp)(O_2CPh)_2](ClO_4)_2 \cdot 2H_2O$, electronic absorption spectrum of $[Fe^{II}Fe^{III}(bimp)(O_2CPh)_2](ClO_4)_2$ in CH_3CN, and cyclic voltammogram of $[Fe^{II}Fe^{III}(bimp)(O_2CPh)_2](ClO_4)_2$ in CH_3CN (21 pages); observed and calculated structure factors for $[Fe^{II}Fe^{III}(bimp)(O_2CPh)_2](BPh_4)_2 \cdot {}^3/_2CH_3CN$ (42 pages). Ordering information is given on any current masthead page.

Small Heteroborane Cluster Systems. 4. The Photochemistry and Organometallic Rearrangement Chemistry of Small Phosphorus-Bridged Borane Cluster Compounds: The Sequential Loss of Boron Vertices from Small Metallaboranes[1]

Bruce H. Goodreau, Lianna R. Orlando,† and James T. Spencer*

Contribution from the Department of Chemistry and the Center for Molecular Electronics, Center for Science and Technology, Syracuse University, Syracuse, New York 13244-4100.
Received May 16, 1991

Abstract: The photochemical decarbonylation and rearrangement of the small phosphorus-bridged, σ-metalated pentaborane(9) cluster $[Fe(\eta^5\text{-}C_5H_5)(CO)_2B_5H_7(\mu\text{-}P(C_6H_5)_2)]$ (**3**) was found to produce the organometallic tetraborane cluster complex $[Fe(\eta^5\text{-}C_5H_5)(CO)B_4H_6(P(C_6H_5)_2)]$ (**4**). The conversion of **3** to **4** was found to be accompanied by the loss of a carbonyl ligand from the iron fragment, the loss of a boron vertex from the cage, and a structural rearrangement to yield the new complex. The structure of complex **4** is based on a substituted *arachno*-pentaborane(11) parent cluster in which one of the BH_2 basal boron atoms has been replaced by an $Fe(\eta^5\text{-}C_5H_5)(CO)(\mu\text{-}PPh_2)$ fragment and a terminal *endo*-hydrogen on the opposite basal boron has been replaced by a diphenylphosphino group. The phosphine is also σ-bound to the iron center in a B–P–Fe bridged mode. Complex **4** was readily converted into the triborane complex $[Fe(\eta^5\text{-}C_5H_5)(CO)B_3H_7(P(C_6H_5)_2)]$ (**5**) through the loss of an additional vertex boron atom by passing **4** down a silica gel column. Both complexes **4** and **5** are relatively air stable materials. A single-crystal X-ray analysis of **5** shows that the structure is based on a substituted *arachno*-B_4H_{10} structure. An alternate description for **5** is based on a metalated $B_3H_8^-$ structure in which the iron fragment coordinates to one boron atom of the $B_3H_8^-$ ligand through a M–H–B interaction and the phosphorus atom bridges between the iron and the adjacent boron atom in much the same fashion as a bridging M–H–B hydrogen atom. Complex **5** represents the first structurally characterized metal triborane complex which exhibits a 1103 *styx* structure. The complete characterization by ^1H, ^{11}B, ^{13}C, ^{31}P NMR, infrared, and mass spectral analyses is reported. Crystallographic data for **5**: space group $P2_1/c$ (No. 14), a = 8.506 (1) Å, b = 14.127 (3) Å, c = 16.121 (3) Å, $\alpha = \gamma = 90.00°$, β = 102.73 (1)°, V = 1889.5 (6) Å^3, Z = 4 molecules/cell.

Introduction

Heteroborane and related heteroatom-bridged cluster compounds, especially the phosphorus-substituted systems, provide convenient models for a wide range of substituted polyhedral cluster systems including the other main group and transition-metal clusters. The relationship between the structures of these clusters and their organometallic chemistry has thus far not been explored in any detail. Very few studies in which the effect of

† National Science Foundation Research Experiences for Undergraduates Participant 1990–1992.

(1) Part 3: Goodreau, B. H.; Ostrander, R. L.; Spencer, J. T. *Inorg. Chem.* **1991**, *30*, 2066.

0002-7863/92/1514-3827$03.00/0